Sofia Peres Coelho
Licenciada em Genética e Biotecnologia

Stereological study on organelle distribution in human oocytes at metaphase-I

Dissertação para obtenção do Grau de Mestre em
Genética Molecular e Biomedicina

Orientador: Doutora Ana Pires-Luís, Professora Auxiliar Convidada, Instituto de Ciências Biomédicas Abel Salazar

Co-orientador: Professor Doutor Mário Sousa, Professor Catedrático, Instituto de Ciências Biomédicas Abel Salazar

Júri:

Presidente: Doutora Maria Alexandra Núncio de Carvalho Ramos Fernandes, Professora Auxiliar da Faculdade de Ciências e Tecnologia da Universidade Nova de Lisboa

Arguente: Doutora Maria de Lourdes Gomes Pereira, Professora Associada com Agregação da Universidade de Aveiro

Março, 2020

FACULDADE DE CIÊNCIAS E TECNOLOGIA
UNIVERSIDADE NOVA DE LISBOA

Stereological study on organelle distribution in human oocytes at metaphase-I

Acknowledgments

First off, I would like to thank everyone who, in some way or another, helped me complete my master's thesis.

I would first like to thank my thesis advisors Dr. Mário Sousa and Dra. Ana Pires-Luís of the Instituto de Ciências Biomédicas Abel Salazar (ICBAS) at Universidade do Porto (UP). They always helped me whenever I had a question about my research or writing. They steered me in the right direction whenever I lost my way.

Likewise, I would like to thank everyone in the Laboratory of Cell Biology, ICBAS-UP, particularly Elsa Oliveira and Ângela Alves, for their help, guidance and kindness.

Special thanks to my boyfriend, Miguel Ribeiro, for being loving, supportive and patient with me during this period of my life. I couldn't have done it without you.

Lastly, big thanks to my friends, particularly Sofia Lemos, and family, especially my parents, for all the love and support throughout the course of my academic journey.

Resumo

A ultrastrutura de ovócitos imaturos parados em metafase-I (MI) humanos é raramente reportada. Quais os organelos mais frequentes e a sua localização são questões ainda sem resposta clara.

O objetivo desta dissertação é descrever a ultrastrutura de ovócitos MI humanos, qualitativamente, descrevendo a sua morfologia, e quantitativamente, analisando estereologicamente volumes relativos (Vv) e distribuição de organelos. A distribuição quantitativa de organelos em ovócitos MI será, ainda, comparada à de ovócitos em profase-I, analisados quantitativamente num estudo anterior.

Ovócitos MI, recolhidos após estimulação ovárica, foram processados para microscopia eletrónica de transmissão, seccionados serialmente e fotografados. Efetuou-se uma análise estereológica usando uma técnica clássica manual baseada em contagem de pontos para calcular Vv ocupados por cada organelo. Testes Kruskal-Wallis e *U*-teste de Mann-Whitney (com correção de Bonferroni) foram usados para comparar Vv ocupados pelos organelos no ovócito inteiro e nas suas três regiões- córtex, subcórtex e citoplasma interno.

Mitocôndrias e elementos do retículo endoplasmático liso (REL) foram os organelos com maior Vv no ovócito inteiro e em cada região. Não foram detetadas diferenças significativas nos Vv de mitocôndrias nem elementos do REL - túbulos, agregados tubulares, vesículas pequenas e vesículas médias - entre as três regiões. Vesículas grandes de REL evidenciaram Vv (P = 0.011) mais elevado no citoplasma interno do que no subcórtex (0.2% *vs* 0%). As vesículas corticais apresentaram Vv (P = 0.004) mais elevado no córtex do que no subcórtex (0.96% *vs* 0.1%) e citoplasma interno (0.96% *vs* 0.1%); vesículas com conteúdo granular denso apresentaram Vv (P = 0.005) mais elevado no córtex do que no subcórtex (0.1% *vs* 0%). Não houve diferenças significativas nos Vv dos dictiossomas e lisossomas.

Estes dados descritivos e quantitativos, combinados com análise semelhante em ovócitos em metafase-II humanos e abordagens moleculares, podem contribuir para melhorar protocolos de estimulação e métodos de maturação *in-vitro*.

Palavras-chave: Ovócitos humanos; ovócitos imaturos; ovócitos em metafase-I, estereologia; ultrastrutura

Abstract

The ultrastructure of metaphase-I (MI) human immature oocytes is largely unreported. Which organelles are more frequent and their location are questions without a comprehensive answer.

The aim of this dissertation is to describe the ultrastructure of MI human oocytes, qualitatively by describing their morphology, and quantitatively, using stereological analysis to analyse the relative volumes (Vv) of each organelle and their distribution. Moreover, the quantitative analysis of organelles in MI oocytes is compared to prophase-I oocytes, quantitatively analysed in a previous study.

MI oocytes, retrieved after ovarian stimulation, were processed for transmission electron microscopy, serially sliced and photographed. Stereological analysis using a classical manual stereological technique based on point-counting was performed to compute relative volumes occupied by each organelle. Kruskal-Wallis test and Mann-Whitney *U*-test (with Bonferroni correction) were used to compare Vv occupied by organelles in the entire oocyte and three oocyte regions – cortex, subcortex and inner ooplasm.

Mitochondria and smooth endoplasmic reticulum (SER) elements are the organelles with highest Vv in the entire oocyte and each oocyte region. No significant differences were detected in Vv of mitochondria and SER tubules, tubular aggregates, small vesicles and medium vesicles among oocyte regions. SER large vesicles show significant higher Vv ($P = 0.011$) in the inner ooplasm than in the subcortex (0.2% *vs* 0%). Conversely, cortical vesicles present significant higher Vv ($P = 0.004$) in the cortex than in the subcortex (0.96% *vs* 0.1%) and inner ooplasm (0.96% *vs* 0.1%); and vesicles with dense granular contents present significant higher Vv ($P = 0.005$) in the cortex than in the subcortex (0.1% *vs* 0%). No significant differences were observed in Vv of dictyosomes and lysosomes.

These descriptive and quantitative data, combined with similar analysis of metaphase-II human oocytes and molecular approaches, could contribute to the improvement of stimulation protocols and *in-vitro* maturation methods.

Keywords: Human oocytes; immature oocytes; metaphase-I oocytes; stereology; ultrastructure

List of Contents

List of Figures

List of Tables

List of Symbols, Abbreviations and Nomenclature

∑A - sum of the areas of all sections of an object

αGs - alpha subunit of G proteins

A_A - partial area

AKT - serine / threonine specific kinase

AL - *annulate lamellae*

AMH - anti-Müllerian hormone

AR - androgen receptor

ART - Assisted Reproduction Treatments

ART - assisted reproductive technologies

aSERT - tubular aggregates

A_T - total area

ATP - adenosine triphosphate

BMP-7 - bone morphogenic protein-7

cAMP - cyclic adenosine monophosphate

CGR - Centro de Genética da Reprodução

cGMP - cyclic guanosine monophosphate

chr - chromosomes

CHUP - Centro Hospitalar Universitário do Porto

CMIN - Centro Materno-Infantil do Norte

COC - cumulus-oocyte complexes

CRE - cAMP response elements

CREB - cAMP response element binding protein

CREM - cAMP responsive element modulator

CV - cortical vesicles

CVar - coefficient of variation

Di - dictyosomes

EGF - epidermal growth factor

ER - endoplasmic reticulum

FF - follicular fluid

FOXO3a - forkhead box O3a

FSH - follicle-stimulating hormone

GC - granulosa cells

GDF-9 - growth differentiating factor-9

GDP - the guanosine diphosphate

GnRH - gonadotrophin-releasing hormone

GPR3 - protein coupled receptor

G-proteins - guanine nucleotide binding proteins

GTP - guanosine-5'-triphosphate

GV - germinal vesicle

GVBD - germinal vesicle breakdown

HGF - hepatocyte growth factor

HMG - human menopausal gonadotropin

ICBAS - Instituto de Ciências Biomédicas Abel Salazar

ICSI - intracytoplasmic sperm injection

IGF-1 - insulin-like growth factor

IT - isolated tubules

IUR - isotropic and uniform random

IVF - *in vitro* fertilization

KGF - keratinocyte growth factor

LH - luteinizing hormone

L_L - partial length

L_T - total length

LV - large vesicles

L_V - length density

Ly - lysosomes

MAPK - activated protein kinase

MI - metaphase-I

MII - metaphase-II

Mi - mitochondria

mp - metaphase-I plate

MPF - M-phase promoting factor

MTOC - microtubular organizer centers

MV - medium vesicles

mv - microvilli

N_V - numerical density

PB1 - first polar body

PCOS - polycystic ovary syndrome

PF - primordial follicles

PI3K - phosphatidylinositide 3-kinase

PKA - protein kinase A

P_P - partial points

PVS - perivitelline space

P_T - possible points

PTEN - tensin homolog

rFSH - recombinant follicle stimulating hormone folitropin

rHCG - recombinant choriogonadotrophin alpha

rLH - recombinant luteinizing hormone

RER - rough endoplasmic reticulum

SEM - standard error of the mean

SER - smooth endoplasmic reticulum

SPM - sperm preparation medium

SRS - systematic random sampling

SV - small vesicles

S_V - surface density

T - section thickness

TEM - transmission electron microscopy

TGFβ - transforming growth factor-β

TICs - theca internal cells

UP - Universidade do Porto

V - smooth endoplasmic reticulum vesicles

VLV - very large vesicles

V_T - total volume

V_V - relative volume

VZ - vesicles containing granular material

VZP - vesicles containing zona pellucida like materials

ZP - zona pellucida

Chapter 1 - Introduction

1.1 - Human Folliculogenesis

The ovarian cortex contains a pool of primordial follicles (PF). Folliculogenesis consists in the recruitment of a PF that then grows and develops into a mature Graafian follicle (Sá and Sousa, 2014), which then has the potential to ovulate and be fertilized, otherwise it dies of atresia. Follicular growth is achieved by cell proliferation and follicular fluid (FF) formation, and its development requires follicle cellular and tissue differentiation (Erickson, 2008). Only about 0.1% of the follicles in the human ovary will achieve differentiation, the rest undergo apoptosis (Sá and Sousa, 2014).

The follicles have different sizes, representing the various stages of folliculogenesis – preantral (primordial, primary, secondary and tertiary) and antral (Graafian) follicle. From primordial to secondary stages the development is gonadotropin-independent and from tertiary to early antral stages the development is gonadotropin-responsive. After that, during follicle recruitment, selection and ovulation, development is gonadotropin-dependent (Sá and Sousa, 2014).

At each menstrual cycle, the ovulating follicle (dominant follicle) originates from a PF that was recruited one year earlier (Sá and Sousa, 2014).

1.1.1 - Folliculogenesis morphology

Follicular development begins at the fourth month of fetal life (Baker, 1963). The number of PF in the ovary determines the reproductive life span of a woman. Ovaries contain up to six millions of germ cells during fetal life. This number decreases to about 300,000 before the first ovulation (puberty). After puberty, entry in growth phase and atresia are processes that result in age-related depletion of the resting follicles (Bomsel-Helmreich *et al.,* 1979).

The primordial follicle (**Fig. 1.1A**) has a diameter of about 25 μm and is composed of an oocyte arrested at the diplotene stage (prophase-I or GV stage) of meiosis, encircled by a single layer of flattened granulosa cells (GC) separated from the stroma by a basal lamina. At this stage, organelles are concentrated around the nucleus (germinal vesicle - GV) (Sá and Sousa, 2014). GCs and the oocyte exist in a microenvironment without contact with other cells. These follicles have limited access to the endocrine system, as the ovarian cortex does not have independent blood supply (Erickson, 2008).

The first major event in folliculogenesis is follicle recruitment - the triggering of an arrested PF to reinitiate development, entering in the pool of growing follicles. Recruitment is pituitary-independent and possibly controlled by autocrine / paracrine mechanisms (Erickson, 2008). This is a continuous

process that begins after PF formation in the fetus and continues throughout the female's life until the pool of PF is depleted (Okutsu *et al.,* 2010). During recruitment some GCs change from a flattened to cuboidal shape. This marks the transition into the primary follicle, accompanied by an increase in oocyte diameter (Li and Chian, 2017), followed by a slow onset of DNA synthesis and the acquisition of mitotic potential in GC, which are indications of recruitment (Erickson, 2008).

The early stages of folliculogenesis can be divided into primary, secondary and early tertiary follicles, based on development of the theca tissue, increased number of GC layers and appearance of a small cavity (antrum) (Erickson, 2008).

The primary follicle (**Fig. 1.1B**) consists of cuboidal GCs arranged in one layer around the oocyte. The change in shape (flattened to cubic) is due to the onset of mitosis, transcription and translation in GCs (Sá and Sousa, 2014). At this stage, cuboidal GCs begin to express follicle-stimulating hormone (FSH) receptors due to activin stimulation. However, in primary follicles the physiological levels of plasma FSH during the menstrual cycle do not influence a GC response, as the number of FSH receptors is low and the flux of FSH is hampered, as the ovarian cortex lacks its own vascular system (Erickson, 2008). The oocyte begins to grow and differentiate, by progressively increasing RNA synthesis, transcribing important oocyte genes, such as those encoding zona pellucida (ZP) glycoproteins. ZP glycoproteins deposit close to the oocyte surface, in the space between the oolema and GCs, forming the ZP, which subsequently encapsulates the oocyte (Erickson, 2008). The ZP consists of a glycoprotein polymer capsule around the oocyte, separating it from the surrounding GCs. It remains with the oocyte until embryo hatching at the blastocyst stage, at the time of embryo implantation (Li and Chian, 2017). Thus, primary follicles start growing by proliferation of GCs and enlargement of the oocyte. The single-layered primary follicles become multilayered secondary follicles (**Fig. 1.1C and 1.2C**) (Li and Chian, 2017). Hence, secondary follicles have two to ten layers of cuboidal GCs forming a multilayered epithelium (Erickson, 2008).

The secondary follicle acquires an outer layer of stroma-like theca cells around the basal lamina, which later differentiates into *theca interna* and *theca externa* (Gougeon, 1998). Theca development is accompanied by angiogenesis and consequent blood flow around the follicle, bringing nutrients and hormones, and removing waste and secretory products from the follicle. At this stage, the oocyte completes its growth when it reaches about 110 μm in diameter, its maximum size. In parallel, the human follicle increases to 2 cm or more in diameter. At the end of this stage, the preantral follicle contains five distinct structural units: a fully grown oocyte surrounded by the ZP, six to ten layers of GCs, the basal lamina, the *theca interna* and the *theca externa* (Erickson, 2008).

The next pre-antral stage, the tertiary follicle (**Fig. 1.1D**), is characterized by the onset of FF secretion. This glycosaminoglycan-rich fluid is secreted by GCs and accumulates in small spaces between them. These spaces merge and a single space is formed in one pole of the follicle, establishing follicle polarity (Sá and Sousa, 2014). This process is called cavitation or beginning of

antrum formation. After cavitation, the basic plan of the Graafian follicle is established and all different cell types are in proper position, ready for proliferation and differentiation (Erickson, 2008).

The antral or Graafian follicle (**Fig. 1.1E**) is an heterogeneous family of somewhat large follicles, from 0.4 to 23 mm, and is characterized by an antrum (cavity) containing FF, from which GCs and the oocyte share a microenvironment rich in regulatory molecules (Edwards, 1974). Five different histological components can be distinguished in the antral follicle: the *theca externa* (mioid cells), the *theca interna* (steroidogenic cells), the GCs surrounded by basal lamina, the FF and oocyte separated from the ZP by the perivitelline space (PVS) (Sá and Sousa, 2014). Despite drastic changes in Graaffian's follicle size, its appearance remains somewhat the same. Its size is determined by the size of the antrum, which in turn is determined by the volume of FF (Erickson, 2008). The connective tissue surrounding GCs differentiates into two distinct cell components. The most external, the *theca externa*, is innervated by autonomic nerves and is formed by mioid cells, which play an important role on ovulation and atresia through their contractile activity. The most internal to GC, the *techa interna*, is formed by a matrix of loose connective tissue rich in small blood vessels. It contains differentiated theca internal cells (TICs). The presence of this vascular bed in the *techa interna* allows the supply of hormones, nutrients, vitamins and cofactors to the GC and the oocyte, thus promoting their growth and differentiation. It should be noted that the luteinizing hormone (LH) receptor is expressed only in *theca interna* (Sá and Sousa, 2014). Theca compartments express their mature phenotype at the beginning of the Graafian follicle, and throughout the life of the follicle no major changes other than those related to vascular and proliferative activities occur (Erickson, 2008).

The GCs form a mass of precisely shaped and positioned cells, arranged in four differentiated GC layers: 1) the outer domain is the membrane granulosa layer, a pseudostratified epithelium of differentiated tall columnar cells, which stop proliferating before the central domains and is maintained by inner layer proliferation; 2) the innermost domain is the periantral granulosa layer, which is in contact with the antral FF; 3) the intermediate domain is the *cumulus oophorus*; and 4) the domain connected to the oocyte is the *corona radiata* (Sá and Sousa, 2014).

Graaffian follicles can be divided in two groups, healthy and atretic. A healthy Graaffian follicle becomes progressively more differentiated until it reaches the preovulatory stage, presenting differential temporal and spatial expression of a large number of genes, which direct cell differentiation, proliferation and FF formation. This process takes about two months in women. In atretic follicles, changes in gene expression prompt oocyte meiosis arrest and apoptosis, as well as GCs apoptosis. Thus, FF accumulation and cell proliferation are responsible for healthy Graaffian follicles growth, while mitosis and meiosis cessation and apoptosis determine Graaffian follicle atresia (Erickson, 2008). About 99.9% of follicles in the ovary degenerate by an apoptotic mechanism triggered in GCs (Sá and Sousa, 2014).

The ovary produces a single dominant follicle at each menstrual cycle destined for ovulation, originating from a pool of small antral follicles at the end of the luteal phase (Sá and Sousa, 2014). The first indication that a dominant follicle is selected appears to be the continuous rapid division of GCs, whereas the proliferation rate decreases in the GCs of the other follicles (Erickson, 2008). Once selected, the dominant follicle continues to grow and the subordinate follicles undergo atresia (Li and Chian, 2017).

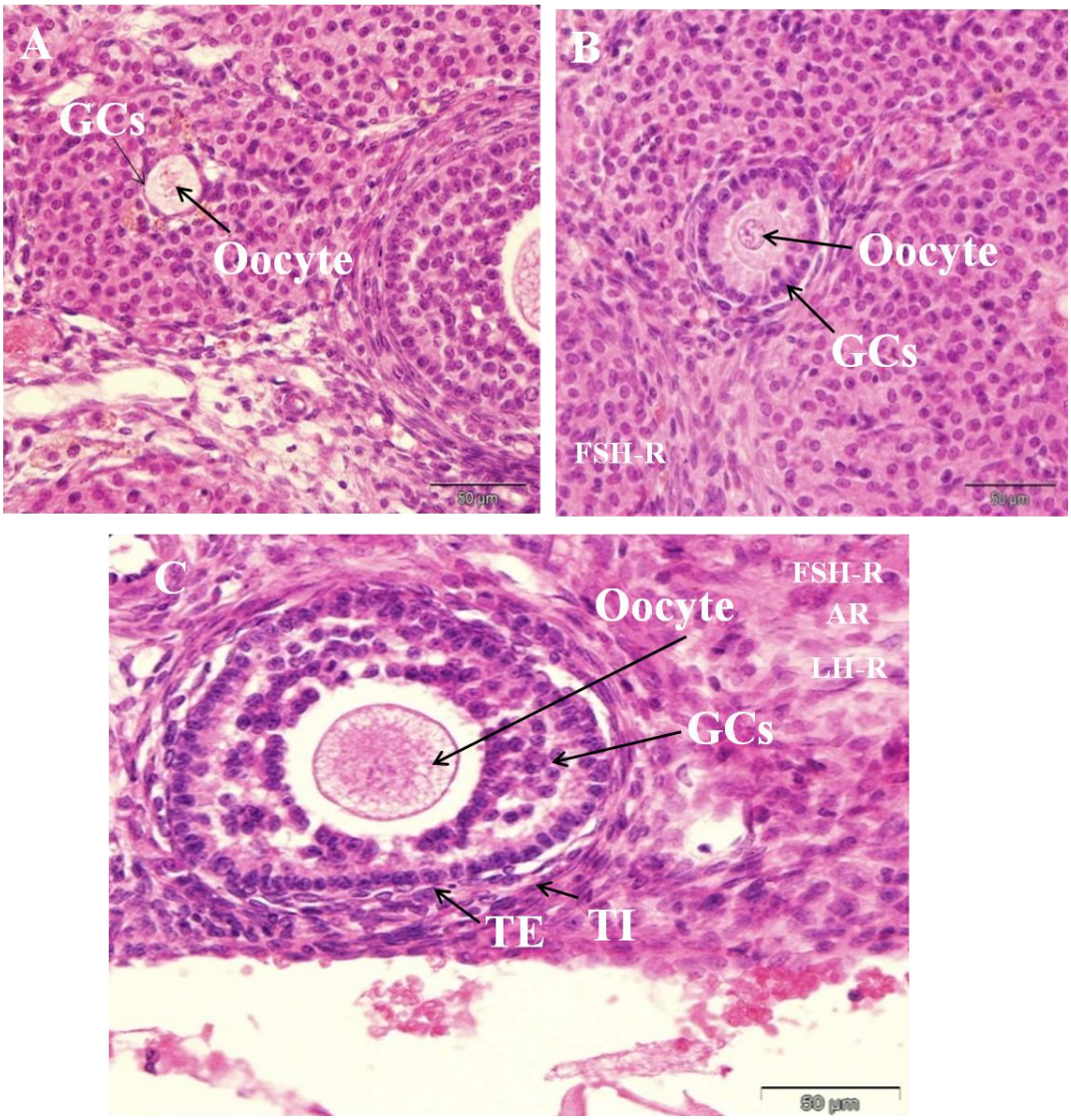

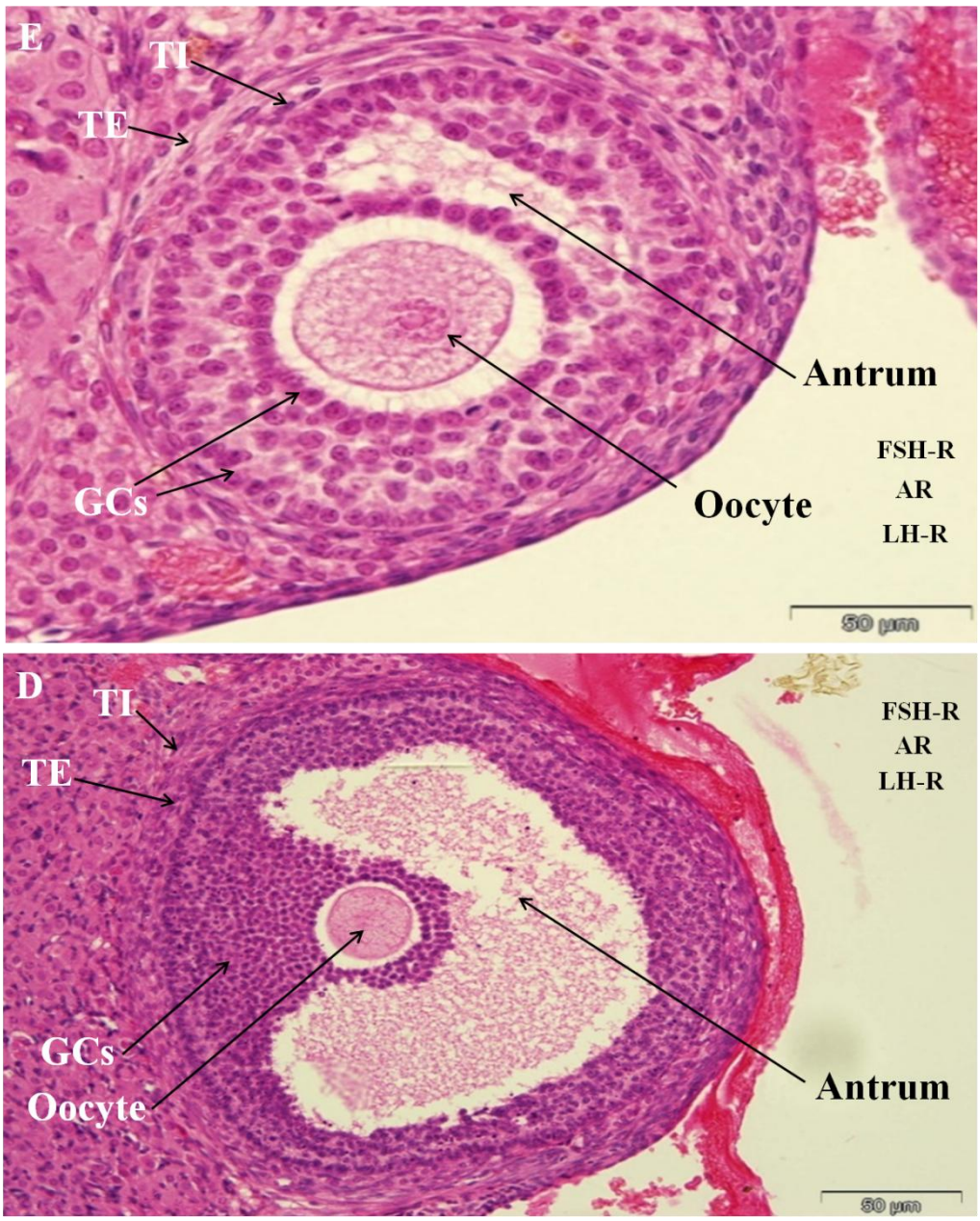

Figure 1.1 - Mouse ovary cortex (illustrative, due to the difficulty in obtaining human ovary cortex images): **A.** Primordial follicle, composed of an oocyte encircled by a single layer of flattened GCs. **B.** Primary follicle, composed of cuboidal GCs arranged in one layer around the oocyte. GCs begin to express FSH receptors. **C.** Secondary follicle, containing two to ten layers of cuboidal GCs. An outer layer of stroma-like theca cells differentiates into *theca interna* and *theca externa*. *Theca interna* cells express the LH receptor. All GCs express FSH receptor at this stage (only represented in some CGs in the figure) and also begin to express the AR receptor. **D**. Tertiary follicle. FF is secreted by GCs and accumulates in small spaces between them beginning antrum formation. **E.** Graffian follicle is characterized by an antrum containing FF, from which GCs and the oocyte share a microenvironment. GCs start to express LH receptors and AR receptors

1.1.2 - Folliculogenesis physiology

Folliculogenesis is regulated by hormones and growth factors that act through autocrine - ligands liberated by a cell that act in the cell itself modulating its activities, such as growth factors, hormones, cytokines and neurotropins - and paracrine – ligands liberated by a cell that act on adjacent cells to modulate their functions - signalling systems (Sá and Sousa, 2014).

Primordial follicles (**Fig. 1.1A**) constitute the total pool of germ cells available during the female reproductive life. They are activated and continuously recruited in cohorts to start folliculogenesis. The phosphatidylinositide 3-kinase (PI3K) signaling pathway is a crucial pathway required for the activation of PF. When this intracellular pathway is activated by growth factors or Kit ligand, a cytokine produced by the GCs of PF, triggers an increase in PI3K that leads to increased phosphorylation of a serine / threonine specific kinase (AKT), resulting in increased cell survival and proliferation, and apoptosis inhibition. Inhibitory factors, such as phosphatises, the tensin homolog (PTEN) and the transcription factor forkhead box O3a (FOXO3a), keep the PI3K pathway under control. PTEN inhibits AKT stimulation, thereby suppressing cell proliferation (Dunlop and Anderson, 2014). In addition, GC expression of anti-Müllerian hormone (AMH), a member of the transforming growth factor-β (TGFβ) superfamily, is necessary to maintain a balance between the number of PF being activated and those remaining in the resting pool, by suppressing PF recruitment (Sánchez and Smitz, 2012).

At the primary follicle (**Fig. 1.1B**) stage, GCs form cytoplasmic expansions that penetrate the ZP and establish gap junctions with the oocyte. This initiates GC control of oocyte growth, keeping the oocyte arrested at prophase-I as cyclic adenosine monophosphate (cAMP) transferred by GCs to the ooplasm inhibits the M-phase promoting factor (MPF) and, thus, meiosis. The metal ion zinc, a secondary messenger, helps to regulate prophase-I arrest through metalloproteinase actions over MPF. At the LH surge, gap junctions are lost due to GCs feet retraction, MPF is activated and the oocyte reinitiates meiosis, first with germinal vesicle breakdown (GVBD), followed by formation of the first meiotic spindle (metaphase-I stage- MI) and, at ovulation, meiosis I completion with extrusion of the first polar body (PB1) and arrest at the second meiotic spindle (mature oocyte stage - MII) (Sá and Sousa, 2014).

At the secondary follicle (**Fig. 1.1C**) stage, GC growth is mediated by the mitogenic action of growth differentiating factor-9 (GDF-9), a member of the TGF-β superfamily secreted by the oocyte. Under LH influence, *theca interna* cells expressing the LH receptor synthesize and secrete androgens, epidermal growth factor (EGF), TGF-α, keratinocyte growth factor (KGF), hepatocyte growth factor (HGF), bone morphogenic protein-7 (BMP-7) and angiogenic factors. These growth factors appear to be important in decreasing apoptosis during the transition from preantral to the early antral stage (Sá and Sousa, 2014). All GCs express FSH receptor at this stage and also begin to express the androgen

receptor (AR). Follistatin, an activin-binding protein, is a small glycoprotein secreted by the pituitary gland known to counterbalance the action of activin on cell proliferation. In combination with BMPs, it stimulates the progression during this transition (Sá and Sousa, 2014).

When the oocyte completes its growth, it acquires the ability to resume meiosis, but oocytes do not usually resume meiosis during folliculogenesis due to inhibitory mechanisms. One proposed mechanism is FSH-induced cAMP synthesis by GCs that then diffuses to the oocyte through the Cx37 gap junction, where it inhibits MPF and thus GVBD (Erickson, 1986).

Cavitation, initiated in the tertiary follicle (**Fig. 1.1D**), is controlled by two growth factors expressed by GCs: activin and KIT ligand (stem cell factor, a cytokine). Activins, which belong to the TGF-β family of growth and differentiation factors, form dimers composed of two β subunits (A and B), induce GC proliferation and are involved in follicular atresia (Orisaka *et al.*, 2009). When cultured GCs are treated with activin, a histological unit with an antrum-like cavity is formed. When KIT ligand action (by binding to the KIT receptor) on GCs is blocked, it prevents the formation of antral follicles, preventing ovulation (Erickson, 2008). Oocyte gap junctions, intercellular channels composed of connexin proteins, also seem important for cavitation. Connexin Cx37 appears to be an oocyte-derived connexion, forming gap junctions between the oocyte and adjacent GCs. These evidences suggest that GC-derived activin, KIT ligand and Cx37 are involved in the autocrine / paracrine mechanisms that control cavitation (Erickson, 2008).

At the Graaffian follicle (**Fig. 1.1E**), GCs of the granulosa membrane layer differentiate as they start to express P450aro, LH receptors, AR and factors that inhibit the expression of pro-apoptotic genes. *Theca interna* only expresses LH receptors and LH regulates the synthesis of androgens and the production of growth factors. The oocyte also contributes to GCs cell differentiation and proliferation by secreting the mitogen GDF-9 (Sá and Sousa, 2014).

FSH is a mandatory induction stimulus for Graaffian follicle growth and development. In its absence, the FF is not produced and no antral follicles develop. A rise in plasma FSH leads to FF accumulation in the microenvironment of one of the follicles in the cohort, destined to be the dominant follicle. FSH receptors are expressed exclusively in GCs, and FSH action is responsible for cell differentiation in the four different GC regions, previously enumerated. Three major responses are induced in GCs: induction of LH receptors, stimulation of division and acquisition of steroidogenic potential (Erickson, 2008).

FSH binds to its receptor with high affinity, initiating a conformational change in the receptor that activates the guanine nucleotide binding proteins (G-proteins), resulting in a cascade of events: the guanosine diphosphate (GDP) bound to the alpha subunit of G proteins (αGs) is phosphorylated to guanosine-5'-triphosphate (GTP); the active αGs-GTP dissociates from the βγ complex; the free-Gs-GTP interacts with adenylate cyclase, generating cAMP; cAMP binds to the regulatory subunits of PKA, causing the complex to dissociate into a dimer of R2 and two free catalytic subunits; the C

subunits phosphorylate the serine and threonine residues of the cAMP response element binding protein (CREB) and cAMP responsive element modulator (CREM) proteins. Following phosphorylation, these proteins can bind to cAMP response elements (CRE), which are upstream DNA regulatory elements, either stimulating or inhibiting gene transcription (Meyer and Habener, 1993).

The dominant follicle produces estradiol, which inhibits a secondary rise of FSH. This leads to subthreshold levels of FSH in nondominant follicles, promoting atresia (Erickson, 2008). Furthermore, if the oocyte does not secrete the growth factor GDF-9 and GCs do not secrete the growth factor granulosa-derived IGF-1 (insulin-like growth factor), antiapoptotic genes are silenced and proapoptotic genes are activated, leading to activation of caspases and apoptosis (Sá and Sousa, 2014).

1.2 - The human ovulated oocyte

Oocytes get ready for fertilization and embryonic development by accumulating essential macromolecules and undergoing genomic modifications as the oocyte grows (Li and Chian, 2017).

Thus, oocyte maturation includes both nuclear maturation, involving resumption of meiosis (completion of the first meiotic division) (Li and Chian, 2017), and cytoplasmic maturation, involving the accumulation of proteins, mRNA, nutrients and substrates, necessary for oocyte maturation, fertilization and early embryogenesis (Watson, 2007). Oocytes are arrested at prophase-I before ovulation. The ovulatory LH surge promotes resumption of meiosis, with progression through the first meiotic division, with extrusion of the PB1 and arrest at the metaphase-II (MII) stage (Sen and Caiazza, 2013).

Throughout the years, the ultrastructure of human oocytes has been reported by several authors, mainly consisting of a slight description on the different developmental stages (Hertig and Adams, 1967; Sundstrom, 1985a,b; Sathananthan, 1985; Yang *et al.,* 2009; Morimoto, 2009; Shahedi *et al.,* 2013; Coticchio *et al.,* 2016; Palmerini *et al.,* 2014; Sousa *et al.,* 2016; Segovia *et al.,* 2017). Regarding GV oocytes, there are a few studies, some presenting a slight structural description (Sathananthan, 1985; Morimoto, 2009; Palmerini *et al.,* 2014). More recently, a study presented a full structural description with a stereological analysis (Pires-Luís *et al.,* 2016). In relation to immature metaphase-I (MI) oocytes, there are a few studies with slight morphological descriptions (Morimoto, 2009; Mao *et al.,* 2014), and case reports on MI arrest during Assisted Reproduction Treatments (ART) (Windt *et al.,* 2001; Levran *et al.,* 2002).

1.2.1 – Cytoplasmic Maturation

Cytoplasmic maturation is the preparation of the oocyte cytoplasm for fertilization and embryonic development. Any defective cytoplasmic maturation can cause a failure to promote male pronuclear formation, increasing chromosomal abnormalities after fertilization (Thibault *et al.,* 1975).

Proteins and RNA molecules accumulate in the oocyte cytoplasm, during growth and folliculogenesis, and are used to sustain the first phase of embryonic development (Li and Chian, 2017). Transcription and storage of maternal mRNA occurs during follicular growth and stops at GVDB. During oocyte maturation, there is an increase in mRNA deadenylation (Watson, 2007).

The reorganization of the oocyte cytoplasm accompanies chromosome condensation and migration. It includes changes in the structure and distribution of cytoplasmic organelles, such as the endoplasmic reticulum (ER), vesicles, dictyosomes (Golgi complexes) and mitochondria. It has been claimed that remodelling and repositioning of these structures is needed for the oocyte to acquire full developmental competence (Conti and Franciosi, 2018).

Organelles, consisting of smooth (SER) and rough (RER) endoplasmic reticulum, *annulated lamellae*, dictyosomes and mitochondria, and structures such as ribosomes and nuages, appear concentrated around the nucleus of GV oocytes. As the oocyte grows, these elements become evenly distributed and finally reorganise at the mature MII stage. In the mature MII oocyte, SER large vesicles and SER tubular aggregates surrounded by mitochondria appear concentrated in the cortical regions, with disappearance of the RER and dictyosomes (Sathananthan, 1994). The presence of nuages evidence a high transcription activity and that of the RER, *annulated lamellae* and ribosomes indicates an active translation activity, all during the first growth phases. This enables oocyte growth and cytoplasmic accumulation that will serve as metabolomic stores (proteins and mRNA) for use after fertilization and during the early embryo cleavages. The main SER functions are protein folding and degradation, lipid metabolism and storage of calcium ions (Mao *et al.*, 2014).

Dictyosomes, made of a stacking of cisterns forming a convex structure, have a central role in many intracellular trafficking events related to protein modification and delivery. Cortical vesicles have been shown to derive from dictyosome membranes during oocyte growth. These small vesicles formed from hypertrophied dictyosomes migrate towards the subcortical region of the oocytes and coalesce to form mature cortical vesicles that later remain under the oolemma (Mao *et al.*, 2014).

Mitochondria are spherical or oval, have a dense matrix and usually evidence transverse or peripheral *cristae* (Sathananthan, 1994). The displacement of mitochondria, whose primary function is adenosine triphosphate (ATP) synthesis, for areas of high energy consumption is crucial for oocyte maturation (Mao *et al.*, 2014). ATP is very important for nuclear and cytoplasmic maturation events, given that spindle formation and chromosomal movements depend on the expression and activity of motor proteins that use ATP as energy source (Duran *et al.*, 2011).

1.2.2 – Nuclear maturation

During nuclear maturation, resumption of meiosis is sequentially characterized by GVBD of prophase-I arrested oocytes, completion of first meiotic division with extrusion of the PB1 and arrest at the metaphase-II stage. Oocyte maturation is initiated by the LH surge (Li and Chian, 2017).

As previously stated, cAMP is the fundamental factor that ensures meiotic arrest before ovulation (Li and Chian, 2017). Oocytes are arrested at prophase-I due to high cAMP concentrations, which maintain a high protein kinase A (PKA) activity. PKA phosphorylates cell cycle components, preventing MPF activation, thus promotig meiotic arrest (Conti and Franciosi, 2018). High cAMP levels were found to be dependent on constitutive activity of a G protein coupled receptor (GPR3) (Nogueira *et al.*, 2006), whose expression has been reported in human oocytes (DiLuigi *et al.*, 2008). In addition, cyclic guanosine monophosphate (cGMP) prevents cAMP degradation. Gap-junction

permeability allows translocation of cGMP from the somatic compartment to the oocyte (Conti and Franciosi, 2018).

The LH surge leads to a block in cGMP production in GCs, which in turn leads to a decrease in cGMP in the oocyte. This causes a decrease in cAMP levels, which triggers the onset of oocyte maturation (Conti and Franciosi, 2018). Furthermore, the mitogen-activated protein kinase (MAPK) is considered pivotal to meiotic arrest regulation in oocytes. Blocking MAPK activity prevents GVBD. MAPK is inactive in human immature oocytes but active in mature oocytes (Li and Chian, 2017).

Lack of or incomplete LH effects, defective signalling in the surrounding GCs, or intrinsic oocyte factors may lead to failure in meiosis resumption (Levran *et al.,* 2002).

After resumption of meiosis, the nucleus migrates to the periphery of the oocyte and chromatin starts condensing. Later on, the nuclear envelope becomes highly folded and fragments, while nucleoli disappear. This is when GVBD occurs. The human oocyte is devoid of centrosomes. Instead, microtubular organizer centers (MTOC) associate with chromosome poles (Sathananthan, 1994). After GVBD the homologous chromosomes arrange at the cell periphery in a barrel shaped typical chromosome spindle, presenting at each pole a MTOC (anastral spindle). The oocyte immediately enters the first meiotic division with separation of the homologous chromosomes between the oocyte and the extruded PB1, while the sister chromatids remain attached (Jones, 2004). The oocyte remains arrested at this metaphase-II stage, with attached sister chromatids arranged in a MII spindle under the oocyte surface.The second meiotic division is completed only at fertilization (Sathananthan, 1994).

Fertilization results in the release of the oocyte from this meiosis II arrest, triggered by an increase in intracellular Ca^{2+} levels. The end of meiosis is marked by the extrusion of the second polar body (Jones, 2005).

1.2.3 – Ultrastructure of human oocytes

Prophase-I oocytes

Under light microscopy, GV oocytes present a roundish shape and are surrounded by a compact ZP. The ooplasm has a homogeneous appearance, with presence of a large visible and eccentrically located nucleus (Sathananthan, 1985; Palmerini *et al.,* 2014). The ooplasm is rich in organelles, which appear concentrated around the nucleus (Palmerini *et al.,* 2014).

By transmission electron microscopy (TEM) observations, the oocyte surface is covered by a continuous layer of long and thin microvilli. Cortical vesicles are spherical and are randomly distributed throughout the ooplasm, being only sporadically present in the oocyte cortex (Morimoto, 2009; Palmerini *et al.,* 2014). However, recent quantitative stereological methods demonstrated that already at the GV stage, cortical vesicles predominate in the oocyte cortex (Pires-Luís *et al.,* 2016). Dense ellipsoidal or sphere-like mitochondria and SER very large vesicles (VLV) predominated in the

inner ooplasm. The other organelles appeared uniformly distributed, namely, dictyosomes, lysosomes, SER large (LV), medium (MV) and small (SV) vesicles, and isolated SER tubules (Pires-Luís *et al.*, 2016) (**Fig. 1.2**). A porous nuclear membrane surrounds a spherical nucleus with one or more dense nucleolar bodies. Small patches of condensed chromatin are sometimes visible close to these bodies (Palmerini *et al.*, 2014).

Two organelles were first described in human GV oocytes by Pires-Luís *et al.*: SER very large vesicles, with elongated and irregular outline appearance, located predominantly in the inner cytoplasm; and medium-sized vesicles presenting floccular fine fibrillar contents most likely corresponding to zona pellucida-like materials. These medium-sized vesicles were not observed in the inner cytoplasm and their structure was very different from that of dense cortical vesicles. Additionally, receptor mediated endocytosis was also identified in GV oocytes (Pires-Luís *et al.*, 2016).

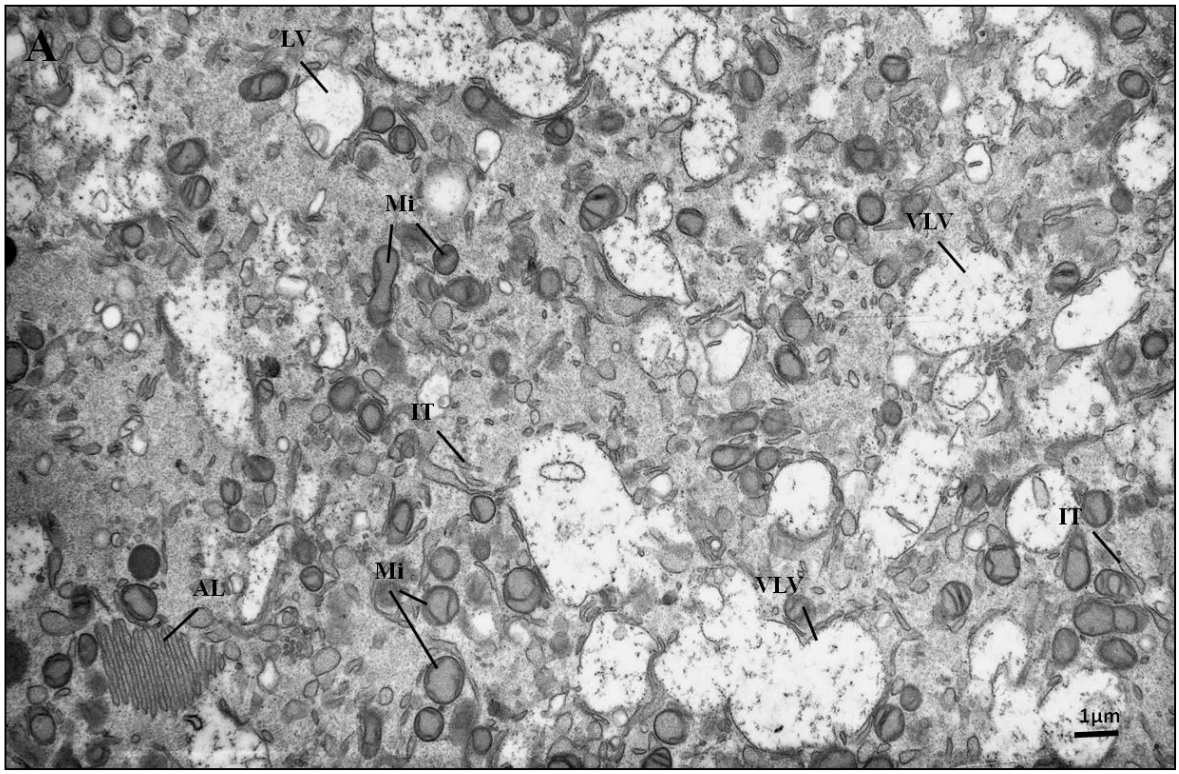

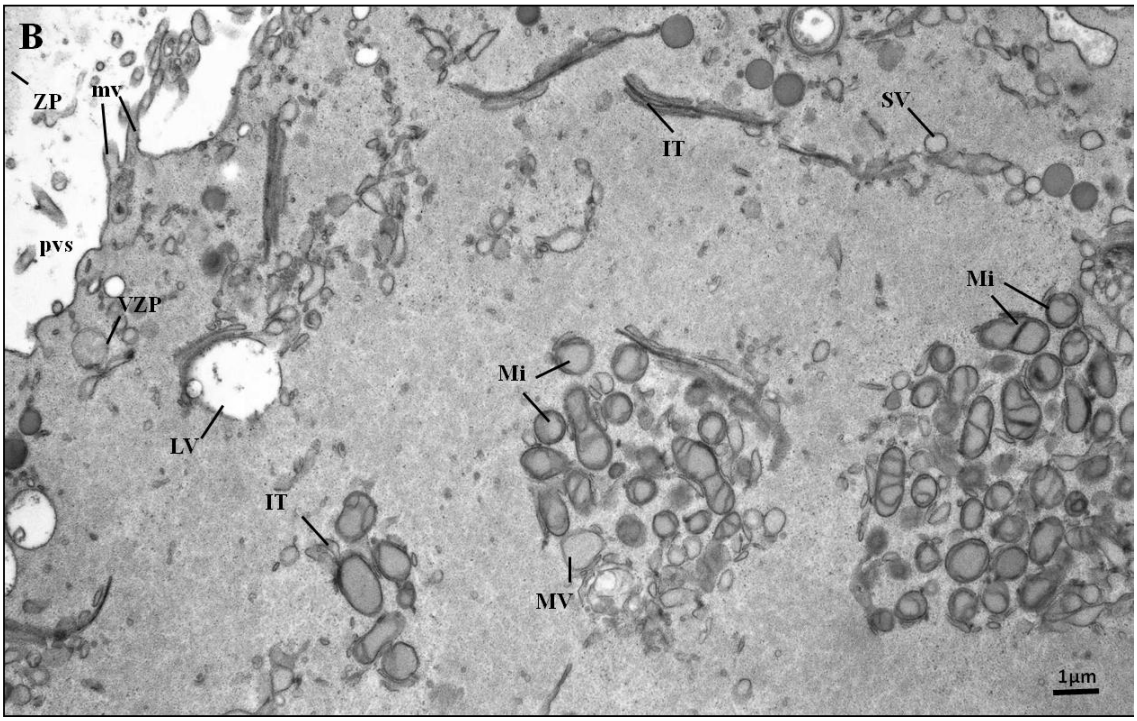

Figure 1.2 - Ultrastructural images of a prophase-I oocyte showing: **A.** Inner ooplasm: mitochondria (Mi), *annulate lamellae* (AL) and smooth endoplasmic reticulum (SER) elements, such as, isolated tubules (IT), large (LV) and very large (VLV) vesicles. **B.** Cortex and subcortex: zona pellucida (ZP), perivitelline space (pvs), microvilli (mv), vesicles containing zona pellucida like materials (VZP), mitochondria (Mi), smooth endoplasmic reticulum (SER) elements, including isolated SER tubules (IT), and SER small (SV), medium (MV) and large (LV) vesicles.

Metaphase-I oocytes

MI oocytes are remarkably bigger than GV oocytes and present higher nuclear area proportion. Microvilli also grow in size and number at this stage (Morimoto, 2009).

At MI stage, the number of mitochondria increases and elongated mitochondria start appearing. Lipid droplets and microfilaments can also be seen. Cortical vesicles increase in number, appear denser and fully migrate towards the cortical ooplasm (Morimoto, 2009; Mao *et al.*, 2014). Some evidence suggests that this process begins at the GV stage (Pires-Luís *et al.*, 2016). SER vesicles grow in size and become more abundant and SER tubules can also be observed. Dictyosomes are rarely observed, being more fragmented and dispersed throughout the oocyte (**Fig. 1.3**) (Morimoto, 2009; Mao *et al.*, 2014).

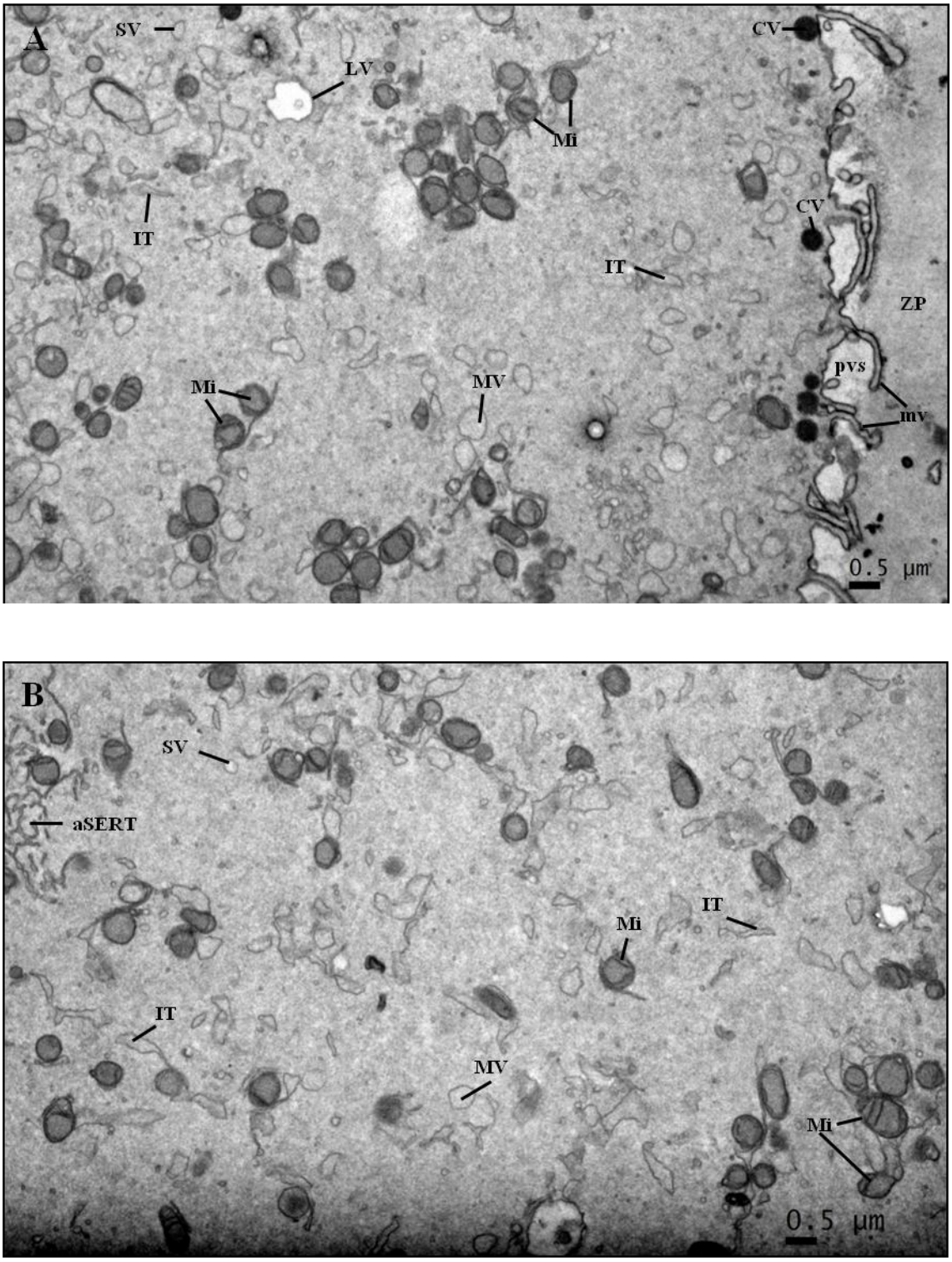

Figure 1.3 - Ultrastructural images of a methaphase-I oocyte showing: **A.** Cortex and subcortex: zona pellucida (ZP), perivitelline space (pvs), microvilli (mv), cortical vesicles (CV), mitochondria (Mi), smooth endoplasmic reticulum (SER) elements, including isolated SER tubules (IT), and SER small (SV) medium (MV) and large (LV) vesicles. **B.** Inner ooplasm: mitochondria (Mi) and smooth endoplasmic reticulum (SER) elements, such as, isolated SER tubules (IT), tubular aggregates (aSERT), and SER small (SV) and medium (MV) vesicles.

Metaphase-II oocytes

MII oocytes exhibit a round shape, a homogeneous ooplasm and a visible PB1. Additionally, they present a continuous ZP consisting of dense fibrilar material, a narrow PVS and large quantity of cytoplasmic organelles, sometimes in clusters (Shahedi *et al.*, 2013; Palmerini *et al.*, 2014).

The oolemma has numerous long and thin microvilli that project into the PVS, being uniformly distributed, except in the zone of polar body extrusion where they are absent. There is a continuous layer of dense round cortical vesicles aligned just underneath the oolemma. Mitochondria and SER elements are the most abundant organelles. Mitochondria are often associated with SER elements (M-SER aggregates), namely SER small and large vesicles in the subcortex and inner cytoplasm, and SER tubular aggregates in the subcortex. Mitochondria are round or ovoid with arc-like or transverse *cristae*, irregularly placed on the periphery and parallel to the outer mitochondrial membrane, and contain a moderately dense matrix (**Fig, 1.4**) (Sousa *et al.*, 1997; Shahedi *et. al.*, 2013; Palmerini *et al.*, 2014; Coticchio *et al.*, 2016).

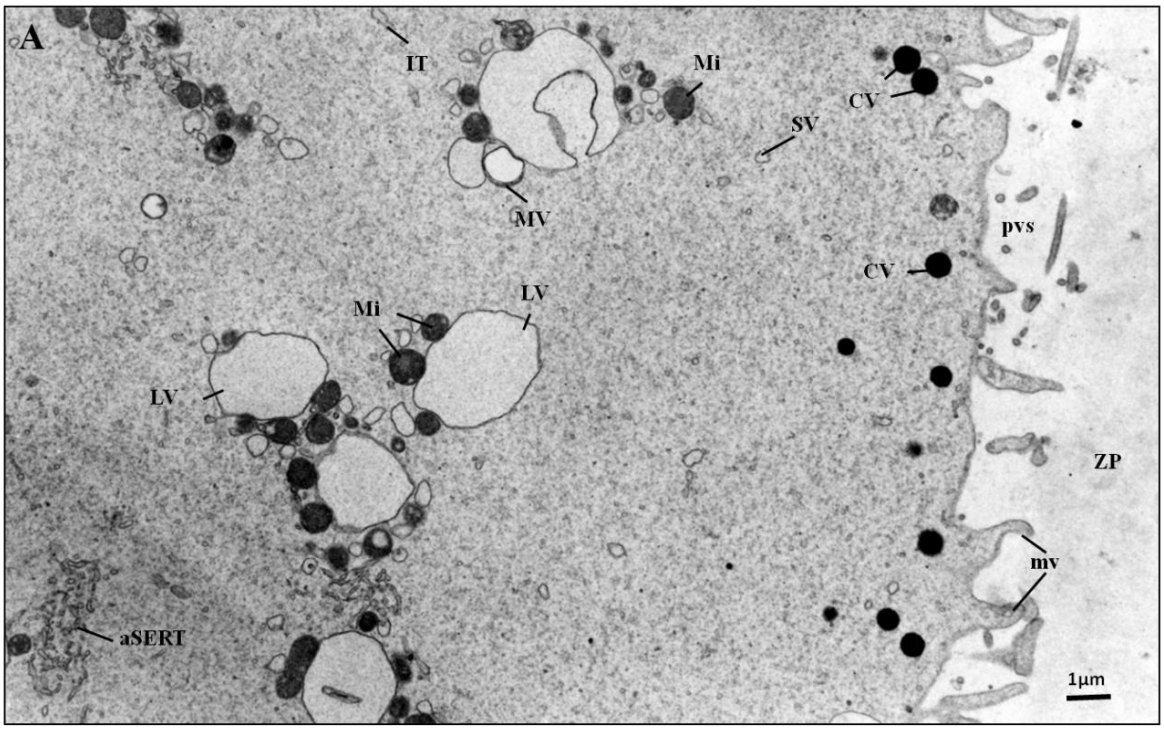

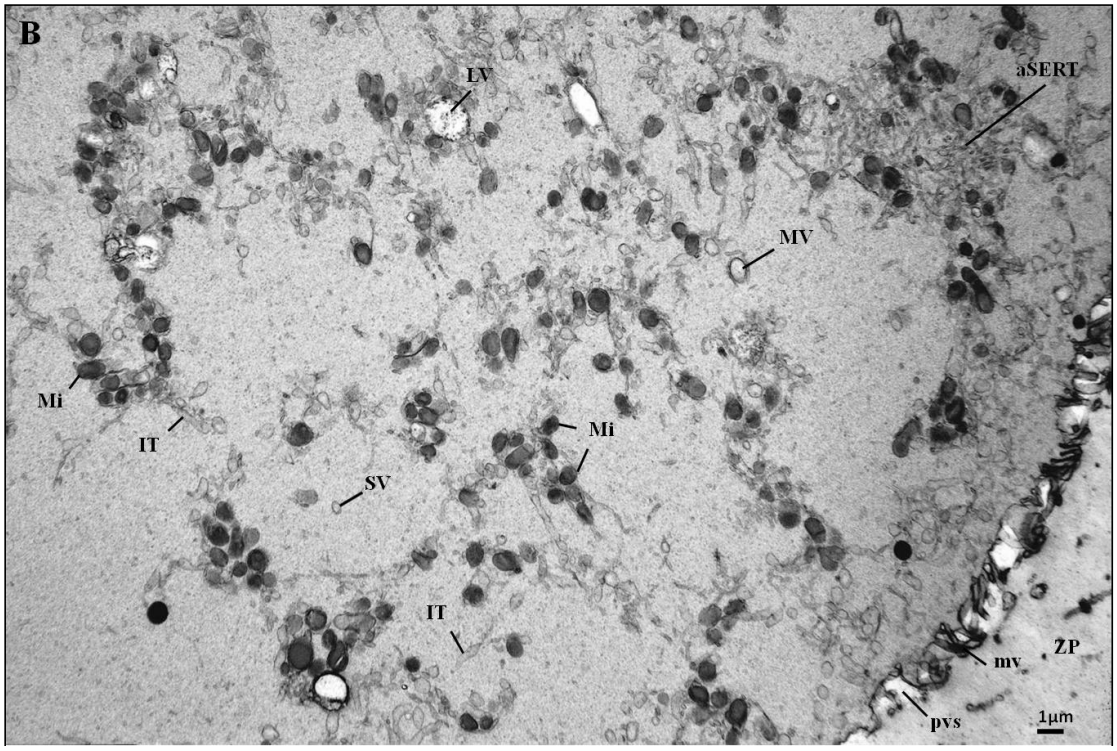

Figure 1.4 - Ultrastructural images of a methaphase-II oocyte showing all three regions (cortex, subcortex and inner ooplasm): **A.** zona pellucida (ZP), perivitelline space (pvs), microvilli (mv), cortical vesicles (CV), mitochondria (Mi), smooth endoplasmic reticulum (SER) elements, including isolated SER tubules (IT), tubular aggregates (aSERT), and SER small (SV), medium (MV) and large (LV) vesicles. **B.** zona pellucida (ZP), perivitelline space (pvs), microvilli (mv), mitochondria (Mi) and smooth endoplasmic reticulum (SER) elements, such as, isolated SER tubules (IT), tubular aggregates (aSERT), and SER small (SV) medium (MV) and large (LV) vesicles..

1.3 - Stereological Methods

Quantitative morphological data facilitates the correlation between structure and function of cells and tissues (Weibel *et. al.*, 1966).

Through stereological methods it is possible to obtain quantitative information about three-dimensional structures contained in two-dimensional sections of these structures, mostly based on observations made on these sections (Gundersen *et al.*, 1988). Fixed and embedded tissues are usually sectioned, which preserves the integrity of the tissue in two of the three dimensions of space, sacrificing the third dimension in favour of better resolution. All structures of the tissue are randomly cut by a non-oriented section. If the sections are very thin in relation to the size of the structures being investigated, thickness may be disregarded and the section can be consider a two-dimensional image of the tissue structure. In these two-dimensional sections, volumes appear as areas, surfaces appear as lines, and lines appear as points (Weibel *et. al.*, 1966).

Sampling is a structured and systematic method that is used in biological studies. Stereological methods are based on systematic random sampling (SRS). The sampling rate is fixed and pre-determined in the first interval. The starting point is a random point of the structure, which provides randomness of sampling, and the sampling continues at the same ratio until the object of interest is exhausted (Howard and Reed, 2005). It has been statistically shown that each point of the structure has an equal sampling chance, so the sampling is homogenous and efficient (Gundersen and Jensen, 1987).

The images of the sections may be obtained by light or transmission electron microscopy (Weibel *et. al.*, 1966).

The number of publications regarding the application of stereology as quantitative tool in biomedical research has largely increased in the last fifty years (Kipanyula and Sife, 2018). Recent articles have shown the use of a stereological approach in studies related to Alzheimer's disease (Furcila *et al.*, 2019), Huntington's disease (Paldino *et al.*, 2019) and Parkinson's disease (Kim *et al.*, 2020), as well as to quantify the total number of white matter interstitial neurons in the human brain (Sedmak and Judas, 2019), to name only a few. Additionally, a study quantifying the distribution of organelles in oocytes at prophase-I using a stereological analysis was performed (Pires-Luis *et al.*, 2016).

1.3.1 - Stereological Principles

Stereological principles provide tools that enable the estimation of densities per volume, such as volumetric density (V_V), surface density (S_V), length density (L_V) and numerical density (N_V), which are the most commonly used. In biology, in order to obtain an estimate of total quantity, these ratios can only be interpreted when combined with an estimate of the total reference volume (volume of the reference space) (Howard and Reed, 2005).

Bonaventura Cavalieri, a mathematician, demonstrated a method for volume estimation. In a serially sectioned structure, cut with a known distance in systematic parallel planes, volume is estimated by summing the areas of all sections of the object ($\sum A$) and multiplying this by section thickness (T). The starting section must be random. The area of the sectional surfaces is estimated by superimposing a point-grid on the sections and counting all points hitting the area of interest, each point representing a unit area (Gundersen *et al.*, 1988; Mandarim-de-Lacerda, 2003; Sagheb and Moudi, 2014). Later on, Delesse, a geologist, devised the Delesse principle, which became the core of stereological thought. It is based on isotropic and uniform random (IUR) sections, where the partial points (P_P) counted on a section and the total of possible points (P_T) is comparable to the ratios between partial and total lengths (L_L and L_T), partial and total areas (A_A and A_T), and partial and total

volumes (V_V and V_T). Thus, volume fractions, area fractions and length fractions of a structure might be estimated by point counting (Mandarim-de-Lacerda, 2003).

Therefore, in order to estimate the volume fraction V_V (volume of the structure/ volume of the specimen) of the structure being studied, P_P (points hitting the structure/points hitting the section) may be used (Gundersen *et al.*, 1988), using the following formula:

$$P_P\,(\text{struct/ref}) = V_V\,(\text{struct/ref})$$

1.3.2- Test systems

In order to get information from the slices, stereological studies need test-systems, composed of a frame, test-points and test-lines (probes). Normally, in test-systems, the total number of points, the line length and test-area are known, which is useful for the estimation of volume density, length density, and surface density (Mandarim-de-Lacerda, 2003), as described above.

To estimate these parameters, a test system ("grid") is placed arbitrarily on random sections. The probes can coincide or not with the structures of interest within the section. Investigators must count only the positive events (when the probe coincides with the structure of interest) and, through appropriate application of the formulae, extract the information required (Weibel *et. al.*, 1966).

A multipurpose test system, which combines lines, points and area, is useful given that it enables the investigator to obtain a large variety of information with only one test system (Weibel *et. al.*, 1966).

Another test-system without lines, composed by cycloid arcs, might be useful with vertical sections and stratified samples if S_V does not need to be estimated (Gundersen *et al.*, 1988).

Test systems may be attached to the microscope's eyepiece, drawn in acetate and put over prints of the sections or over the monitor screen in video microscopic systems (Mandarim-de-Lacerda, 2003).

Objective of this thesis

The aims of this study are:

1) Qualitative analysis of human arrested MI oocytes, by describing their morphology;

2) Quantitative analysis of human arrested MI oocytes, by using a stereological approach to quantify the relative volume (Vv) of each organelle and its distribution;

3) Comparison of organelle relative volume (Vv) and distribution between human arrested MI oocytes and GV oocytes.

This work was based in:

Sofia Coelho, Ana Sílvia Pires-Luís, Elsa Oliveira, Ângela Alves, Carla Leal, Mariana Cunha, Márcia Barreiro, Alberto Barros, Rosália Sá, Mário Sousa (2020) Stereological study of organelle distribution in human oocytes at metaphase I. Accepted in *Zygote*: Manuscript ID ZYG-2019-0122 DOI: 10.1017/S0967199420000131

Chapter 2 - Materials and Methods

2.1 - Ethical approval

Ethical guidelines were followed in the conduction of the research, with written informed consent obtained before experiments. This work did not involve experiments in humans or animals. We used donated samples of surplus immature oocytes. The approval of the Ethics Committee and the Declaration of Helsinki, revised in Tokyo 2004, on human experimentation does not apply to this work. The private infertility clinic Centro de Genética da Reprodução (CGR) and of the *in vitro* fertilization (IVF) unit of the Public Hospital Centro Materno-Infantil do Norte - Centro Hospitalar Universitário do Porto (CMIN-CHUP) procedures are under the determinations of the National Law on Medically Assisted Procreation (Law of 2017) and supervised by the National Council on Medically Assisted Procreation (CNPMA-2018). According to these rules and guidelines, the use of clinic databases and patient biological material for diagnosis and research can be used without further ethical approval, under strict individual anonymity and after patient informed and written consent.

Regarding the use of immature oocytes in laboratorial experimentation (processing for electron microscopy) at Instituto de Ciências Biomédicas Abel Salazar – Universidade do Porto (ICBAS-UP), the Ethics Committee authorization number is Project: 2019/CE/P017 (266/CETI/ICBAS).

2.2 - Patients

We performed this research using five arrested MI oocytes retrieved after controlled ovarian stimulation during ART treatments performed at CGR and CMIN-CHUP.

2.3 - Ovarian controlled hyperstimulation

Women underwent controlled ovarian hyperstimulation with a gonadotrophin-releasing hormone (GnRH) antagonist protocol (0.25 mg cetrorelix, Cetrotide; Merck-Serono, London, UK; or 0.25 mg ganirelix, Orgalutran; MSD, Hertfordshire, UK); or with a long agonist protocol (0.1 mg triptorelin, Decapeptyl; Ipsen Pharma Biotech, Signes, France). For stimulation, recombinant follicle stimulating hormone (rFSH, folitropin beta, Puregon; MSD, Haalem, Netherlands; or rFSH, folitropin alfa, Gonal-F; Merck-Serono) was used, alone or in combination with human menopausal gonadotropin (HMG, Menopur; Ferring, Kiel, Germany) or recombinant luteinizing hormone (rLH lutropin alfa + rFSH folitropin alfa, rLH+rFSH, Pergoveris, Merck-Serono; or rLH, Luveris, Merck-Serono). In some cases,

it was used only HMG. Ovulation trigger was performed with recombinant choriogonadotrophin alpha (rHCG, 250 µg, Ovitrelle; Merck-Serono), with a GnRH agonist (0.2 mg triptorelin), or with a dual trigger, using triptorelin (0.2 mg) and rHCG (250 µg). The assays of estradiol serum levels were at the day of HCG or one day before (Huirne *et al.*, 2007; Pinto *et al.*, 2009).

2.4 - Gamete and embryo handling

Procedures were performed on a K-Systems laminar flow with thermal base (Cooper Surgical, Malöv, Denmark). For IVF, cumulus-oocyte complexes (COC) were collected in SynVitro Flush medium (without heparin, Origio, Malöv, Denmark). All media were devoid of phenol red. After this step, gamete handling was performed under paraffin oil (Ovoil-100, Vitrolife, Frölunda, Sweeden). COC were washed with SynVitro Flush medium in 1-well culture dishes (Falkon, Corning, New York, NY, USA). They were then transferred to an ESCO incubator (MRI-6A10, EscoMedical, Singapore, Singapore) (37ºC, 5% O_2, 6% CO_2, 89% N_2, in a humidified atmosphere) with Sequential Fert (Origio) and incubated for 2 h. Thereafter they were denuded for 30 sec, with recombinant hyaluronidase (ICSI Cumulase, Origio), washed with sperm preparation medium (SPM) and then mechanically dissociated from granulosa cells in SPM (Origio) with oocyte denudation micropipettes (Vitrolife). Denudation was performed at 37ºC (thermic laminar flow base). After denudation, immature oocytes were transferred to Falcon tubes (Falcon) containing SPM and processed for TEM.

2.5 - Transmission electron microscopy

Oocytes were fixed with Karnovsky (2.5% glutaraldehyde, 4% paraformaldehyde, 0.15 M sodium cacodylate buffer) (Sigma-Aldrich, St. Louis, USA; Merck, Darmstadt, Germany) at room temperature during 30 min. After washing in 0.15 M sodium cacodylate buffer, pH 7.3 (Merck) for 2 h at 4ºC, oocytes were post-fixed with 2% osmium tetroxide (Merck) in buffer containing 0.8% potassium ferricyanide (Merck) for 2 h at 4°C. After washing in buffer (10 min), oocytes were serially dehydrated in ethanol (Panreac, Barcelona, Spain), equilibrated with propylene oxide (Merck) and embedded in Epon (Sigma). Semi-thin and ultra-thin sections were prepared with a diamond knife (Diatome, Hatfield, Switzerland) in a LKB ultramicrotome (Leika Microsystems, Weltzlar, Germany). A Random Numbers Table was used for the selection of first sampling levels. After the first level, MI oocytes were serially sectioned and sampled each 15 µm. In each sampling level, ultrathin sections were collected on 100-mesh formvar carbon-coated copper grids (Taab, Berks, UK) and stained with 3 % aqueous uranyl acetate (20 min) (BDH, Poole, UK) and Reynolds lead citrate (10 min) (Merck).

Ultrathin sections were observed under a JEOL 100XII transmission electron microscope (JEOL, Tokyo, Japan) operated at 60 kV (Sousa and Tesarik, 1994; El Shafie *et al.*, 2000).

2.6 – Quantitative (stereological and statistical) analysis

For each oocyte sampling level, a systematic sampling was performed: after random first field selection, photographs were taken at alternate TEM field spaces when more than 50% of the field was occupied by the oocyte. Photos were taken at ×5300 magnification and printed at 20.2 cm x 20.2 cm. A classical manual stereological technique based on point-counting with an adequate stereological grid was used (**Fig. 2.1A**). Printed photographs were placed under the grid and the number of grid points placed over each organelle was noted (**Fig. 2.1B**). The relative volume (Vv) of each organelle was obtained by applying the formula Vv (organelle, oocyte) = [number of points (organelle)/number of points (oocyte)] × 100 (%) as previously described (Weibel *et al.*, 1966). All measures were performed in the printed version. The organelles included in the evaluation were: cortical vesicles (CV), vesicles containing granular material (VZ), mitochondria (Mi), dictyosomes (Di), lysosomes (Ly), SER tubular aggregates (aSERT), SER isolated tubules (SER-IT), SER small vesicles (SER-SV: smaller than mitochondria), SER medium vesicles (SER-MV: more or less the size of mitochondria), SER large vesicles (SER-LV: larger than mitochondria), and Total SER (SV, MV, LV, IT, aSERT).

In addition, each oocyte was divided into three regions from the oolema up to the cell centre: cortex (5 µm), subcortex (5-10 µm) and inner cytoplasm (> 10 µm). The same stereological procedure was then adopted, applying the formula:

Vv (organelle, cortex/ subcortex/inner cytoplasm) = [number of points (organelle)/number of points (cortex/subcortex/inner cytoplasm)] × 100 (%) (Pires-Luís *et al.*, 2016).

Statistical analysis was performed with Microsoft Excel 2007 and SPSS version 22.0 (IBM Corp, Foster City, California, CA, USA). Results are presented as means, standard error of the mean (SEM = standard deviation/$n^{1/2}$) and coefficient of variation (CVar = standard deviation/mean).

Normal distribution was tested with Kolmogorov-Smirnov test. As the samples did not follow a normal distribution, non-parametric tests were used. Kruskal-Wallis test and Mann-Whitney *U*-test with Bonferroni correction were used to compare the means of Vv (organelle, oocyte), Vv (organelle, cortex), Vv (organelle, subcortex) and Vv (organelle, inner cytoplasm). Statistical significance level was set at $P < 0.05$.

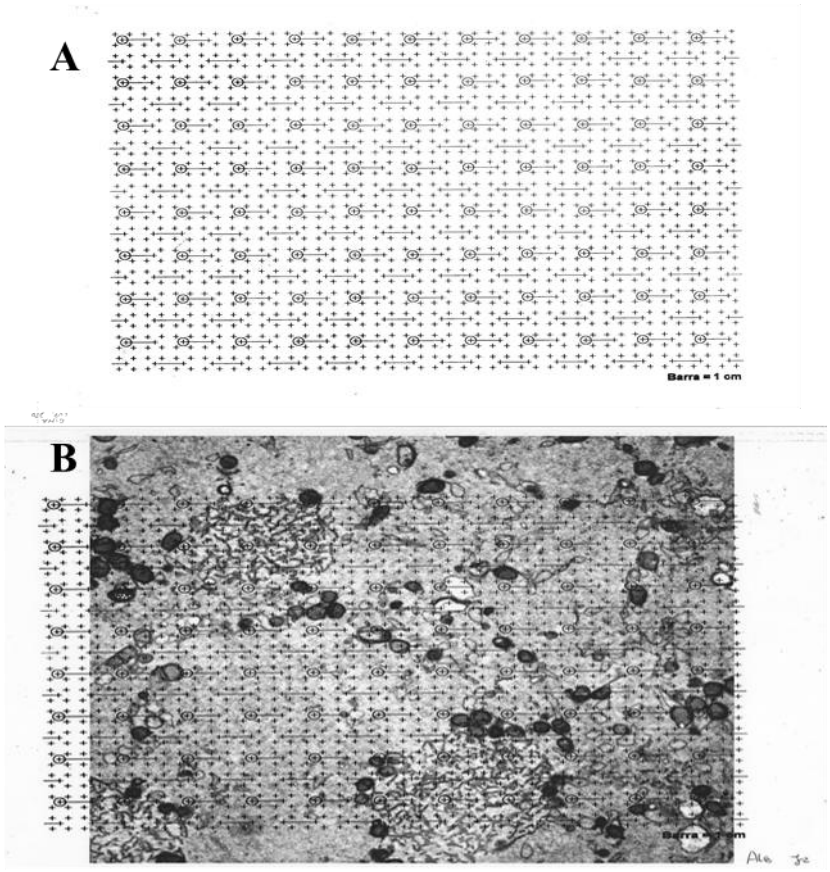

Figure 2.1- A. Stereological grid. **B.** Micrograph region with an overlapping stereological grid.

Chapter 3 – Results

3.1 – Qualitative (morphological) analysis

The overall appearance of the oocyte cytoplasm (ooplasm) and its surface was noted on semi-thin sections (**Fig. 3.1A/B**). MI oocytes are roundish cells surrounded by a thick and translucent ZP. Between the ZP and the cell membrane there is the PVS, a short and narrow space with follicular cell feet remnants and projected microvilli from the oocyte membrane (oolema). Under the oolema, cortical vesicles were observed. The remainder ooplasm contains mitochondria and lucent vesicles, which appeared homogeneously distributed. Some large areas in the oocyte cytoplasm, predominantly at the cortex and subcortex, were bare of major organelles. Close to the surface and eccentrically placed, the metaphase-I plate was observed.

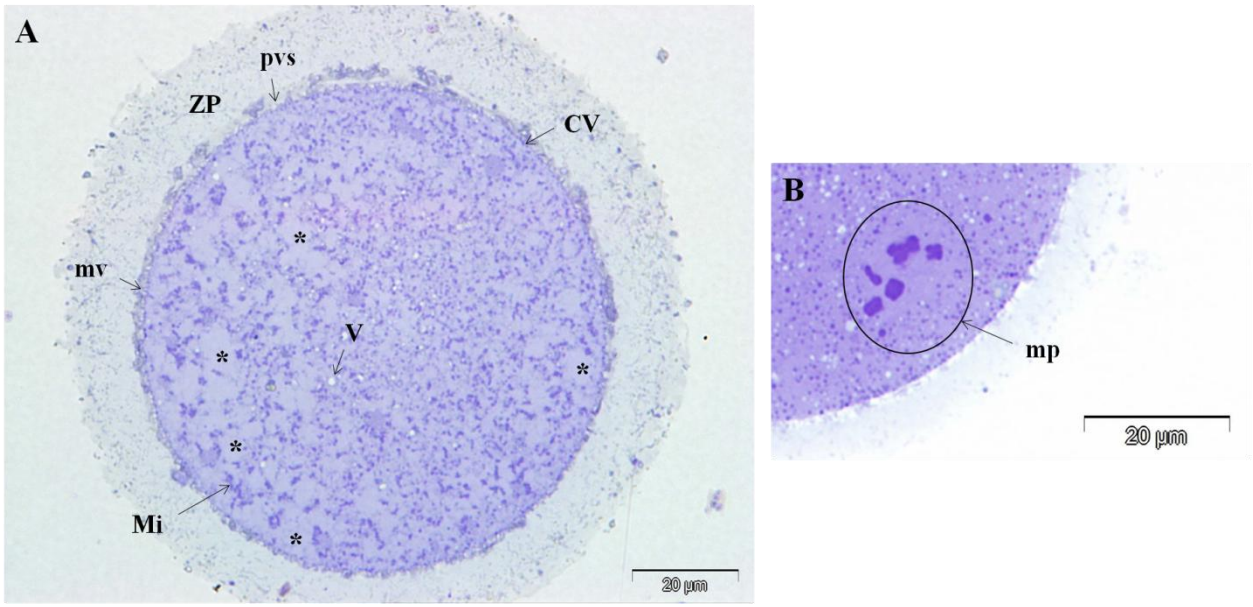

Figure 3.1- Semithin sections of a MI oocyte. **A.** The oocyte is separated from the zona pellucida (ZP) by the perivitelline space (pvs), containing microvilli (mv). The oocyte cortex presents cortical vesicles (CV). The ooplasm shows mitochondria (Mi), smooth endoplasmic reticulum vesicles (V) and areas devoid of major organelles (*). **B.** The metaphase-I plate (mp) extends from the cortex to the inner region.

These observations were corroborated by ultrastructural analysis (**Fig. 3.2A/B/C and Fig. 3.3A/B/C/D**). A narrow PVS separating ZP and the oocyte membrane was observed in ultra-thin sections, as well as long and narrow microvilli, coated-vesicles and coated-pits at the oocyte surface. Cortical vesicles were dense and formed a continuous row along the oocyte surface, under the oolema, and a few isolated cortical vesicles were present in the subcortex and inner cytoplasm. Some medium-

sized vesicles containing dense granular materials (VZ) were observed mostly in the cortex and occasionally appeared to fuse with the oolema, expelling their contents into the perivitelline space. Dispersed in the oocyte cytoplasm, several mitochondria were noted with variable size, mainly oval, with moderately dense matrix and thin and dense *cristae* mostly perpendicular to the organelle membrane - some isolated, some associated with SER vesicles or tubules and some as part of aggregates. Dictyosomes were rare, very small and composed of a few narrow *cisternae* – without evidence of activity at *Cis* or *Trans* faces. Secondary lysosomes varied in size and contents. Several SER components were found - SER-SV, SER-MV, SER-LV, SER-IT and SER aSERT, the last ones often associated with mitochondria. The ooplasm also presented a network of areas devoid of organelles, mostly in the subcortex. The metaphase-I plate was observed crossing all three oocyte regions starting from the oocyte cortex. Centrioles, *annulate lamellae*, rough endoplasmic reticulum, multivesicular bodies, lipid droplets or polyribosomes were not observed. As cytochemical analyses were not performed, the presence of primary lysosomes or peroxisomes could be excluded. The metaphase-I plate (mp) extended from the cortex to the inner region (**Fig. 3.4**).

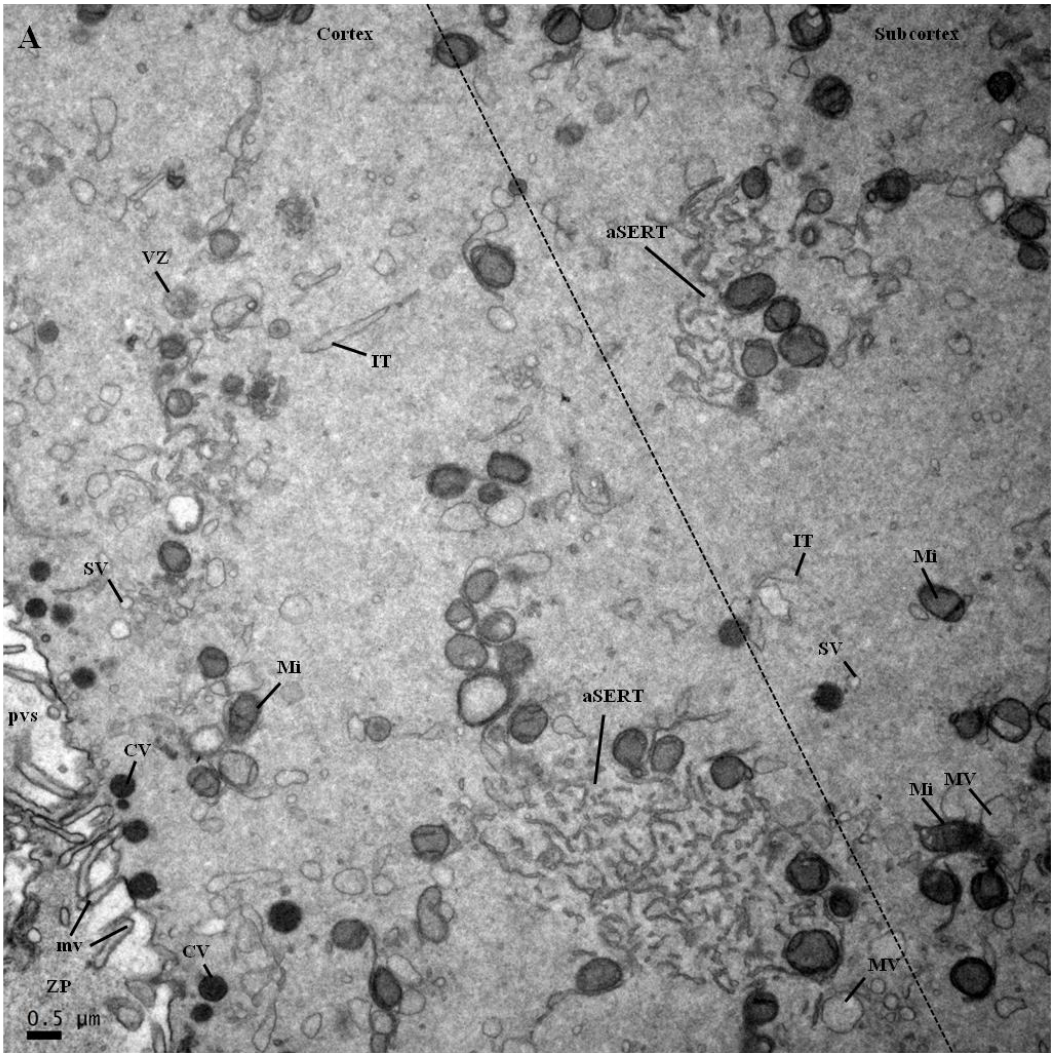

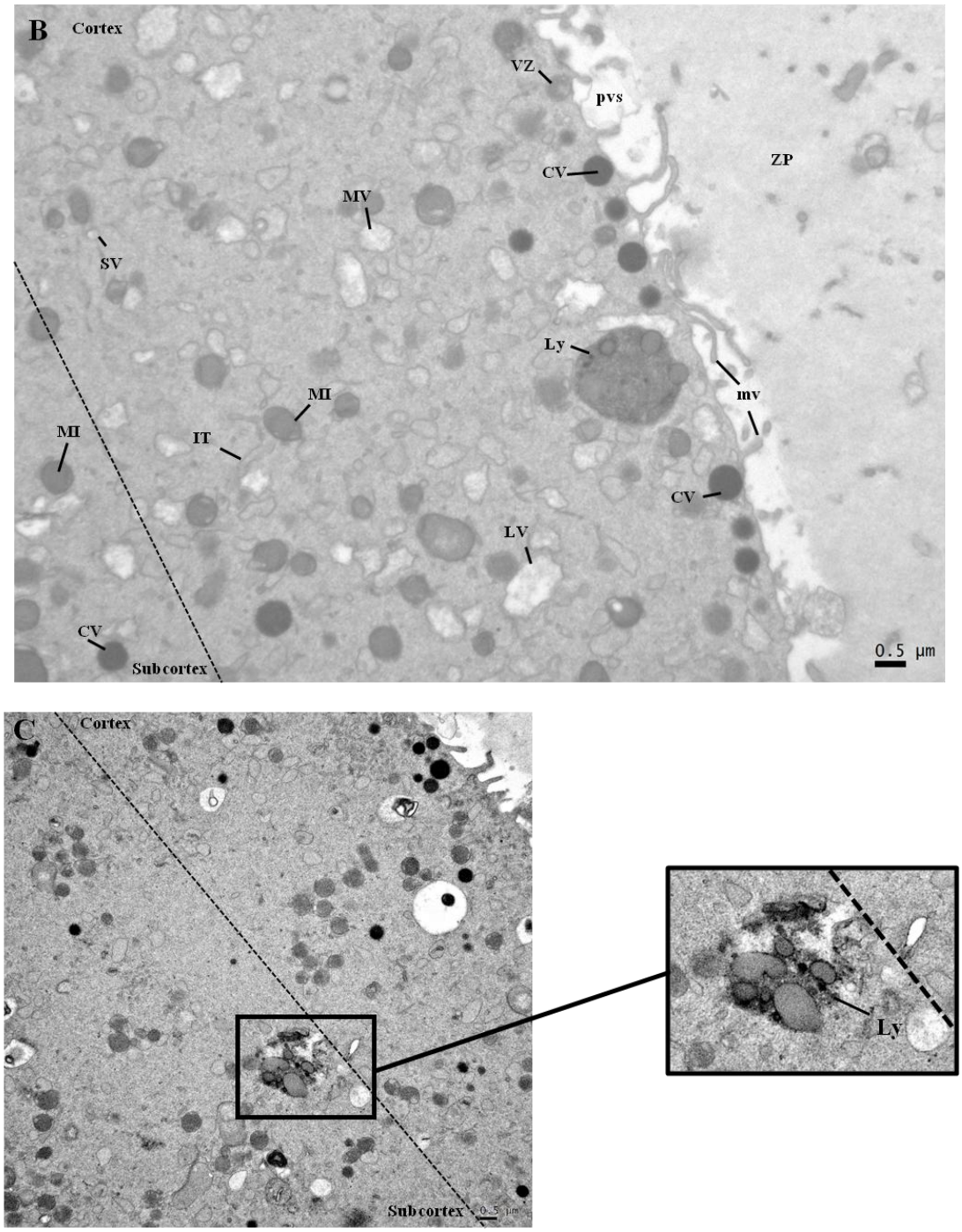

Figure 3.2- Ultrastructural images of metaphase-I oocytes showing the cortex and the subcortex. The distinct regions are separated by dotted transversal lines (5 µm from the oocyte membrane). **A/B.** Between the oocyte and the zona pellucida (ZP) is the perivitelline space (pvs), containing microvilli (mv). Cortical vesicles (CV) are mostly present in the cortex under the oolema. Mitochondria (Mi) and smooth endoplasmic reticulum elements, including isolated tubules (IT) and small (SV) and medium (MV) vesicles, are found in these two regions. Smooth endoplasmic reticulum large (LV) vesicles are present in the oocyte cortex but not in the oocyte subcortex. A lysosome (Ly) is also shown in the oocyte cortex. **C.** Close up of a lysosome (Ly) present in the oocyte subcortex.

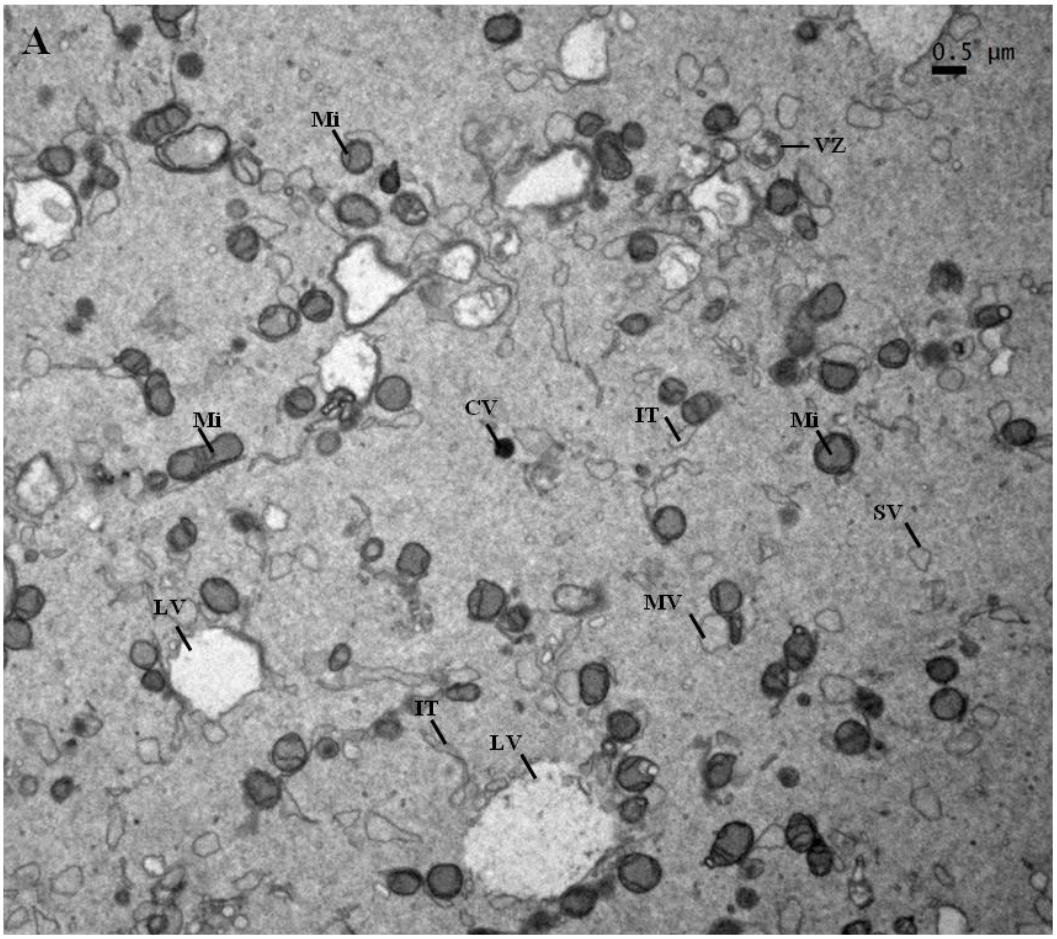
A
0.5 μm
Mi
VZ
Mi
CV
IT
Mi
SV
LV
MV
IT
LV

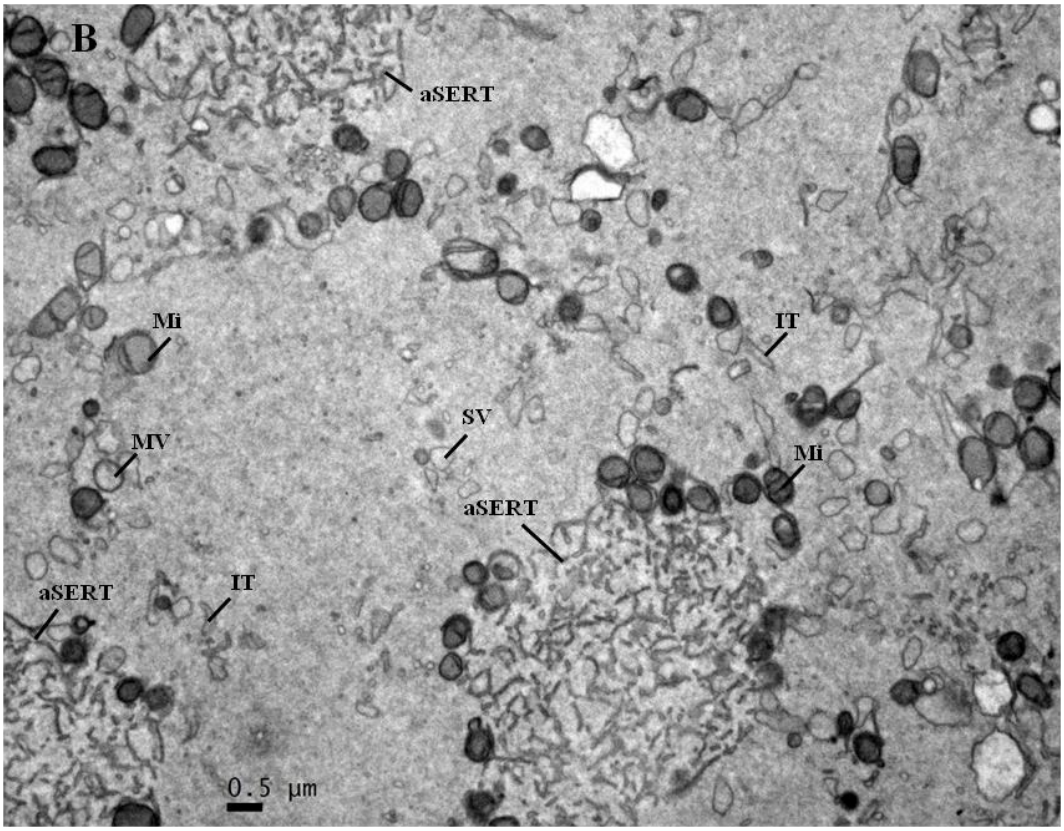
B
aSERT
Mi
IT
SV
MV
Mi
aSERT
aSERT
IT
0.5 μm

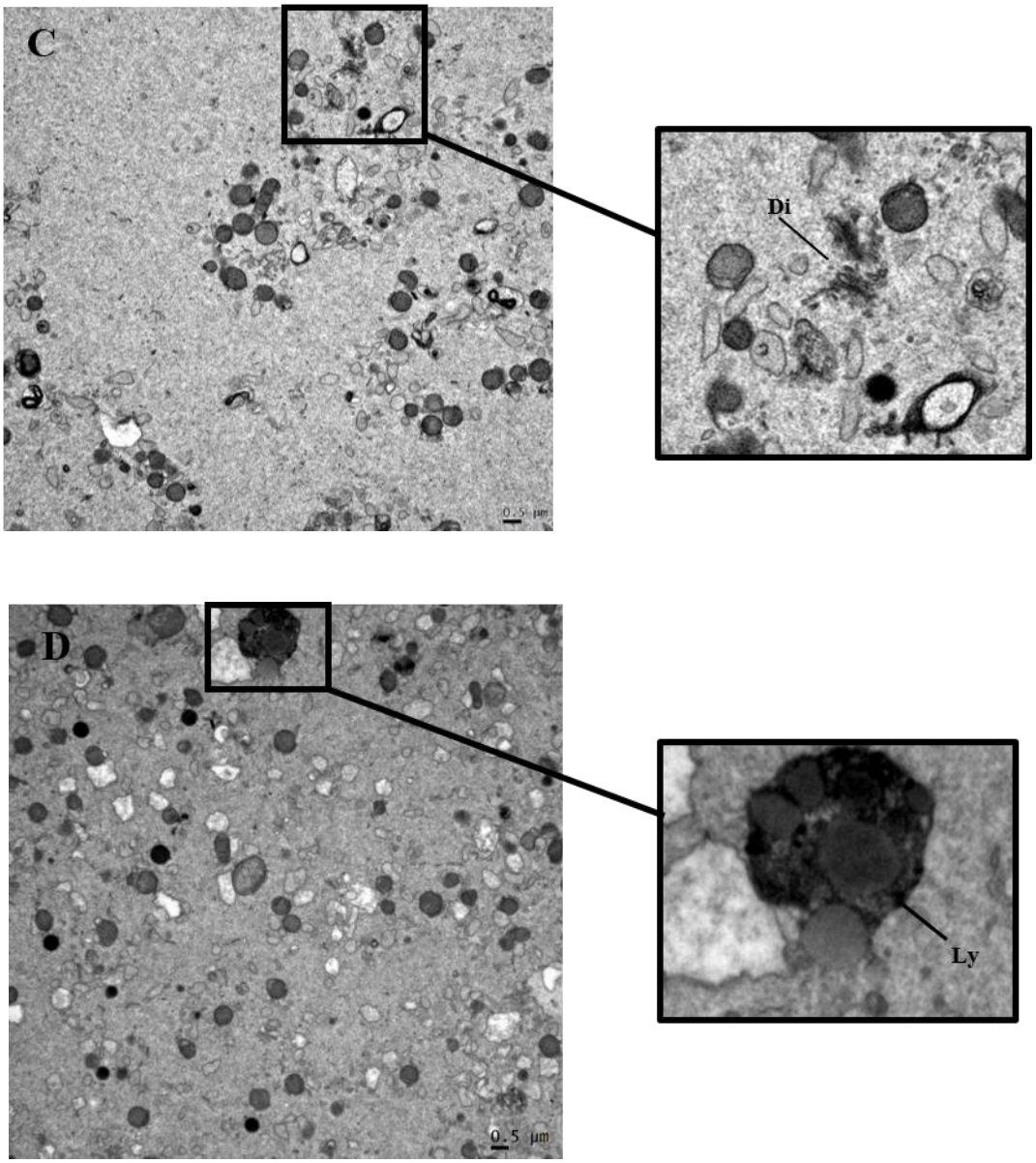

Figure 3.3- Ultrastructural images of metaphase-I oocytes showing the inner ooplasm. **A/B.** The ooplasm evidences numerous mitochondria (Mi) and smooth endoplasmic reticulum elements, such as tubular aggregates (aSERT), isolated tubules (SER-IT), small (SER-SV), medium (SER-MV) and large (SER-LV) vesicles. A cortical vesicle (CV) and a VZ vesicle (VZ) are also observed. **C/D.** Close ups of dictiosomes (Di) and a lysossome (Ly), respectively.

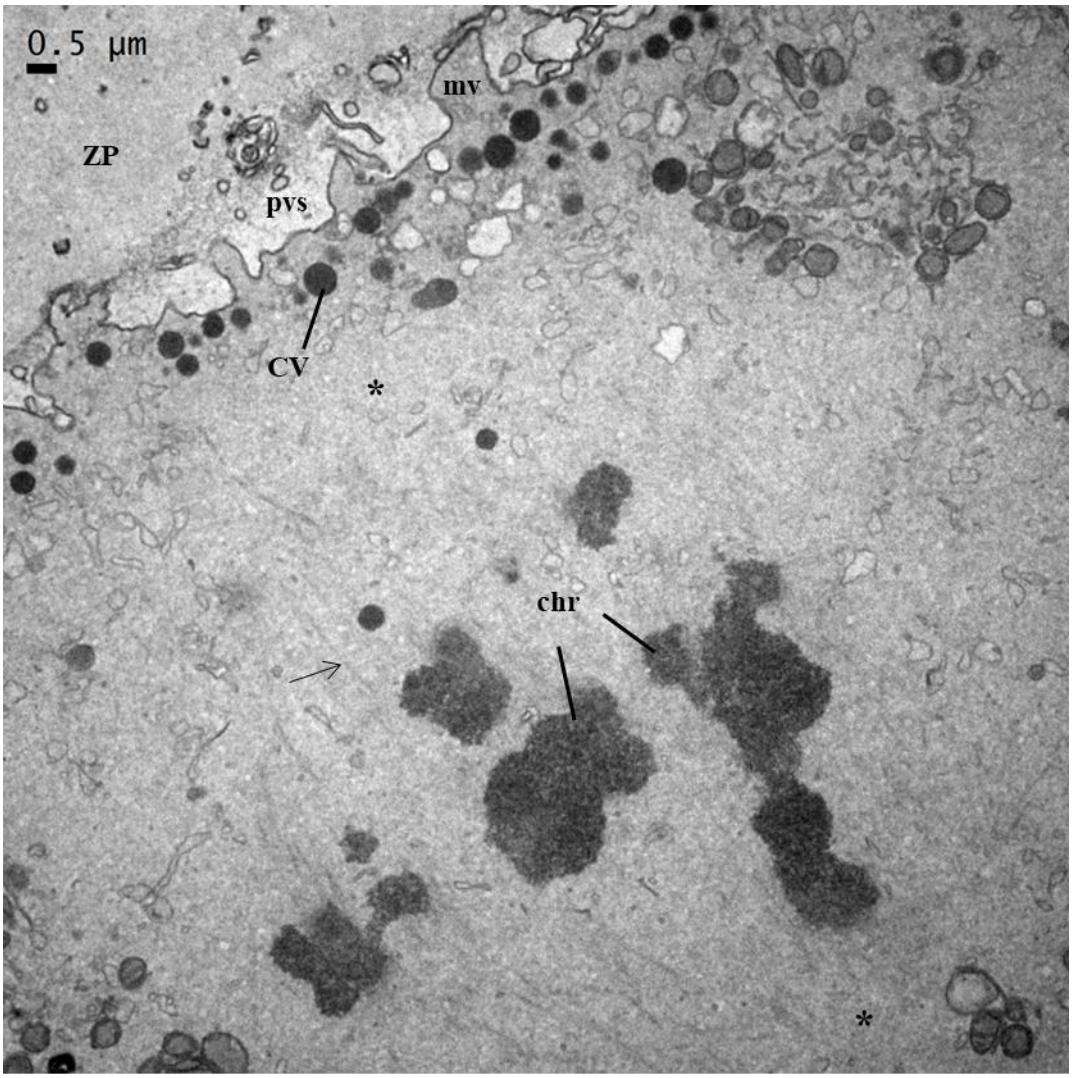

Figure 3.4- The metaphase-I plate. Zona pellucida (ZP), perivitelline space (pvs), microvilli (mv), cortical vesicles (CV), chromosomes (chr), spindle microtubules (arrows). The spindle is anastral (*).
.

3.2 – Quantitative (stereological) analysis

A total of 320 photographs were analysed, 153 representing the oocyte cortex, 142 representing the oocyte subcortex and 167 representing the oocyte inner cytoplasm.

By quantitative analysis, mitochondria and SER elements were the organelles that occupied the highest mean relative volumes in the ooplasm, with Vv (mitochondria, oocyte) = 6.5% and Vv (total SER, oocyte) = 15.05%. Among SER elements, isolated tubules (Vv = 9.4%) and medium vesicles (Vv = 4.5%) predominated. The remainder quantified organelles occupied mean relative volumes lower than 1% each - cortical vesicles (Vv = 0.04%), VZ vesicles (Vv = 0.04%), dictyosomes (Vv = 0.01%), lysosomes (Vv = 0.4%), aSERT (Vv = 0.8%), SER small vesicles (Vv = 0.2%) and SER large vesicles (Vv = 0.2) (**Table1**).

When the mean relative volumes of organelles were compared among oocyte regions (cortex, subcortex and inner ooplasm), it was observed that cortical vesicles predominated in the oocyte cortex (Vv = 0.96%) compared to the subcortex (Vv = 0.1%) and inner ooplasm (Vv = 0.1); VZ vesicles were mostly found in the oocyte cortex (Vv = 0.1) and rarely in the inner ooplasm (Vv = 0.01%); mitochondria were similarly distributed throughout the three oocyte regions (cortex: Vv = 6.3%; subcortex: Vv = 7.3%; inner ooplasm: Vv = 6.4%); dictyosomes were rarely observed in the cortex and inner ooplasm (Vv = 0.01% for both); and lysosomes were evenly distributed throughout the cortex (Vv = 0.3%), subcortex (Vv = 0.3%) and inner ooplasm (Vv = 0.4%). Regarding SER elements, aSERT were mostly found in the cortex (Vv = 1.02%) and subcortex (Vv = 1.3%) compared to the inner ooplasm (Vv = 0.6%); SER-IT were frequently observed and regularly distributed in the cortex (Vv = 10.4%), subcortex (Vv = 9.6%) and inner ooplasm (Vv = 8.8%), with a small progressive decrease from the cortex to the inner region; SER-SV were regularly distributed in all three regions (Vv = 0.2%); SER MV had a slightly higher mean relative volume in the inner ooplasm (Vv = 4.7%) than in the cortex (VV = 4.1%) and subcortex (VV = 3.5%); and SER-LV were mainly found in the inner ooplasm (Vv = 0.2%) and rarely observed in the cortex (Vv = 0.07%). Summarizing, SER-IT, SER-MV and mitochondria were the most predominant organelles in each oocyte region. Cortical vesicles and VZ vesicles were mostly found in the cortex, aSERT were mainly found in the cortex and subcortex, whereas SER-LV were mostly observed in the inner ooplasm (**Table1**).

Table 3.1 - Relative volume of organelles (Vv) per MI oocyte, oocyte cortex, subcortex and inner ooplasm. Results are presented as mean (%), SEM: standard error of the mean (standard deviation/$n^{1/2}$), and CVar: coefficient of variation (standard deviation/mean).
CV: cortical vesicles; VZ: vesicles with dense granular material; Mi: mitochondria; Di: dictyosomes; Ly: lysosomes; SER: smooth endoplasmic reticulum; aSERT: SER tubular aggregates; SER-IT: SER isolated tubules; SER-SV: SER small vesicles; SER-MV: SER medium vesicles; SER-LV: SER large vesicles.

Organelle	Vv (organelle, oocyte) mean (%) ± SEM (CVar)	Vv (organelle, cortex) mean (%) ± SEM (CVar)	Vv (organelle, subcortex) mean (%) ± SEM (CVar)	Vv (organelle, inner ooplasm) mean (%) ± SEM (CVar)
CV	0.4 ± 0.07 (0.42)	0.96 ± 0.17 (0.39)	0.1 ± 0.03 (0.49)	0.1 ± 0.03 (0.82)
VZ	0.04 ± 0.03 (1.49)	0.1 ± 0.07 (1.58)	0	0.01 ± 0.005 (1.67)
Mi	6.5 ± 0.59 (0.20)	6.3 ± 0.23 (0.08)	7.3 ± 0.39 (0.12)	6.4 ± 0.86 (0.30)
Di	0.01 ± 0.004 (0.91)	0.01 ± 0.01 (1.63)	0	0.01 ± 0.006 (1.28)
Ly	0.4 ± 0.09 (0.57)	0.3 ± 0.08 (0.71)	0.3 ± 0.13 (0.95)	0.4 ± 0.11 (0.57)
aSERT	0.8 ± 0.25 (0.69)	1.02 ± 0.33 (0.72)	1.3 ± 0.46 (0.80)	0.6 ± 0.22 (0.86)
SER-IT	9.4 ± 0.50 (0.12)	10.4 ± 0.42 (0.09)	9.6 ± 0.46 (0.11)	8.8 ± 0.59 (0.15)
SER-SV	0.2 ± 0.06 (0.68)	0.2 ± 0.07 (0.73)	0.2 ± 0.08 (0.79)	0.2 ± 0.06 (0.68)
SER-MV	4.5 ± 1.003 (0.50)	4.1 ± 1.18 (0.64)	3.5 ± 1.02 (0.64)	4.7 ± 0.96 (0.45)
SER-LV	0.2 ± 0.06 (0.91)	0.07 ± 0.03 (1.05)	0	0.2 ± 0.1 (1.02)
Total SER (SV, MV, LV, IT, aSERT)	15.05 ± 1.25 (0.19)	15.9 ± 1.27 (0.18)	14.6 ± 1.35 (0.21)	14.5 ± 1.38 (0.21)

The three oocyte regions – cortex, subcortex and inner ooplasm - were compared with the Kruskal-Wallis test (**Table 2**). Significant differences were observed in the mean relative volume occupied by cortical vesicles, VZ vesicles and SER-LV among these areas. No differences were detected in the mean relative volume occupied by mitochondria, lysosomes, dictyosomes, SER-SV, SER-MV, SER-IT, total SER vesicles, SER tubules and aSERT among these areas.

Furthermore, for Vv (cortical vesicles, oocyte), Vv (VZ vesicles, oocyte) and Vv (SER-LV, oocyte), strict pairwise comparisons were performed with the Mann-Whitney *U*-test (with Bonferroni correction) for the three regions - cortex vs subcortex, cortex vs inner ooplasm, subcortex vs inner ooplasm (**Table 2**). Significant differences were observed in the mean relative volume occupied by

cortical vesicles (cortex > subcortex > inner ooplasm), VZ vesicles (cortex > subcortex) and SER-LV (inner ooplasm > subcortex).

Table 3.2 - Comparison of the means of Vv (organelle, cortex), Vv (organelle, subcortex) and Vv (organelle, inner ooplasm) in MI oocytes.
CV: cortical vesicles; VZ: vesicles with dense granular materials; Mi: mitochondria; Di: dictyosomes; Ly: lysosomes; SER: smooth endoplasmic reticulum; aSERT: SER tubular aggregates; SER-IT: SER isolated tubules; SER-SV: SER small vesicles; SER-MV: SER medium vesicles; SER-LV: SER large vesicles. *Significant *P* value significant at $p<0.05$.

Organelle	**Kruskal-Wallis** (*P* value*)	**Mann-Whitney** (*P* value*)	
CV	**0.004**	Cortex vs. Subcortex (Vv 0.96 vs 0.1)	**0.008**
		Cortex vs. Inner ooplasm (Vv 0.96 vs 0.1)	**0.008**
VZ	**0.005**	Cortex vs. Subcortex (Vv 0.1 vs 0)	**0.008**
Mi	0.432		
Di	0.182		
Ly	0.754		
aSERT	0.468		
SER-IT	0.061		
SER-SV	0.811		
SER-MV	0.403		
SER-LV	**0.011**	Subcortex vs. Inner ooplasm (Vv 0 vs 0.2)	**0.008**
Total SER	0.756		

3.3 – Comparison between GV and MI oocytes

The relative volume of each organelle was also compared between MI oocytes and the results previously obtained in GV oocytes (Pires-Luís *et al.*, 2016), as the study on GV oocytes shares a similar design and classification criteria regarding the present methodology.

In relation to morphology, rough endoplasmic reticulum, lipid droplets and polyribosomes were not observed in GV nor MI oocytes. Vesicles containing zona-pellucida-like materials, multivesicular bodies, *annulate lamellae* and SER-VLV, which were observed in GV oocytes, were absent in MI

oocytes. In opposition, VZ vesicles, aSERT and associations between mitochondria and SER elements were not present in GV oocytes but were observed in MI oocytes.

Regarding quantitative data, in GV oocytes, the the top three organelles with higher Vv were SER-VLV (localized mainly in the inner ooplasm), mitochondria and total SER elements. In MI oocytes, the same findings were observed for mitochondria and total SER.

The relative volume of each organelle was also compared between GV and MI whole oocyte ooplasm, and for each oocyte region – GV cortex *vs* MI cortex, GV subcortex *vs* MI subcortex, GV inner ooplasm *vs* MI inner ooplasm (**Table 3**).

We found that the mean relative volumes occupied by dictyosomes and SER-SV were significantly higher in GV oocytes, whereas SER-IT, SER-MV and total SER were significantly higher in MI oocytes. Additionally, significant differences were detected in the mean relative volumes occupied by mitochondria in the oocyte cortex (higher in MI oocytes) and SER-LV in the oocyte subcortex (higher in GV oocytes). No significant differences were detected between the relative volume occupied by cortical vesicles, mitochondria, lysosomes and SER-LV.

Table 3.3 - Comparison of the means of Vv (organelle, cortex-c), Vv (organelle, subcortex-sc) and Vv (organelle, inner ooplasm -ic) between GV oocytes and MI oocytes.
GV: prophase-I oocytes (germinal vesicle stage); MI: metaphase-I oocytes; CV: cortical vesicles; Mi: mitochondria; Di: dictyosomes; Ly: lysosomes; SER: smooth endoplasmic reticulum; aSERT: SER tubular aggregates; SER-IT: SER tubules; SER-SV: SER small vesicles; SER-MV: SER medium vesicles; SER-LV: SER large vesicles.
*Significance set at $P < 0.05$
** Data is presented as the Vv found in the different organelles in GV oocytes (from Pires-Luís et al., 2016), the comparative *P* value between the Vv of GV vs MI oocytes for each organelle, and the Vv found in the different organelles in MI oocytes (from Table 1).

Organelle	Vv (organelle, oocyte) GV vs MI GV (*P* value)*, MI**	Vv (organelle, cortex) GV vs MI GV (*P* value) MI	Vv (organelle, subcortex) GV vs MI GV (*P* value) MI	Vv (organelle, inner ooplasm) GV vs MI GV (*P* value) MI
CV (Vv)	0.3 (0.612) 0.4	1.3 (0.268) 0.96	0.1 (0.530) 0.1	0.1 (0.432) 0.1
Mi (Vv)	6.3 (0.089) 6.5	3.6 (**0.01**) 6.3	6.0 (0.073) 7.3	7.2 (0.530) 6.4
Di (Vv)	0.5 (**<0.001**) 0.01	0.4 (**0.003**) 0.01	0.6 (**0.010**) 0	0.6 (**0.003**) 0.01
Ly (Vv)	0.2 (0.067) 0.4	0.1 (0.202) 0.3	0.1 (0.432) 0.3	0.3 (0.639) 0.4
SER-IT (Vv)	3.2 (<**0.001**) 9.4	3.3 (**0.005**) 10.4	3.2 (**0.003**) 9.6	3.1 (**0.003**) 8.8
SER-SV (Vv)	2.5 (<**0.001**) 0.2	2.0 (**0.003**) 0.2	2.3 (**0.003**) 0.2	2.7 (**0.003**) 0.2
SER-MV (Vv)	0.2 (<**0.001**) 4.5	0.1 (**0.003**) 4.1	0.2 (**0.003**) 3.5	0.3 (**0.003**) 4.7
SER-LV (Vv)	0.2 (0.072) 0.2	0.07 (0.876) 0.07	0.1 (**0.010**) 0	0.2 (0.876) 0.2
Total SER (Vv)	6.1 (<**0.001**) 15.05	4.6 (**0.003**) 15.9	5.8 (**0.003**) 14.6	6.23 (**0.003**) 14.5

Chapter 4 – Discussion

An oocyte needs to attain competence to be fertilised. This process is called oocyte maturation. It involves cytoplasmic maturation, where the oocyte prepares for fertilization and embryonic development by accumulating RNA molecules, proteins, substrates and nutrients in the cytoplasm as it grows. These are then used to sustain the early phase of embryonic development (Watson, 2007). It also involves nuclear maturation, consisting in the resumption of meiosis - the first meiotic division is completed and the second division is arrested at the metaphase-II stage until fertilization. This is prompted, during each reproductive cycle, by a pre-ovulatory LH surge, which initiates disassembly of the nuclear envelope – GVBD, followed by chromosomal condensation, spindle formation, and extrusion of the first polar body. Then, the oocyte initiates the second meiotic division and becomes arrested at metaphase-II stage until fertilization. After fertilization, it resumes meiosis and extrudes the second polar body, and nuclear maturation is completed (Mehlmann, 2005).

Numerous studies on oocyte maturation have been reported throughout the years, using different methodologies, such as: microarray analysis (Wood *et al.,* 2007), genome analyses (Hou *et al.,* 2013), gene expression profiling (Virant-Klun *et al.,* 2013), characterization of the essential genes for human oocyte maturation (Liu *et al.,* 2016), single-cell proteomics (Virant-Klun *et al.,* 2016), genome-wide, single-cell DNA methylomics (Yu *et al.,* 2017), characterization of calcium oscillations (Ferrer-Buitrago, 2018), characterization of growth hormones promoting in vitro maturation (Li *et al.,* 2019) and single-cell transcriptomics (Zhao *et al.,* 2019), illustrating the relevance of this topic and the recent expansion of molecular data on oocyte maturation, which might be useful for clinical practice.

Indeed, all around the world, millions of oocytes are harvested and then cultured every year to provide ART for infertile couples (Mandelbaum, 2000). It has been shown that human oocytes are able to mature *in vitro* when isolated from follicles and placed in appropriate culture medium (Edwards, 1965 a,b). The first successful IVF of human oocytes matured *in vitro* was reported in 1969 (Edwards *et al.,* 1969) and the first successful human pregnancy from IVF of oocytes retrieved from natural ovulatory cycles was reported in 1978 (Steptoe and Edwards, 1978). The successful fertilization, development and pregnancy using *in vitro* matured human oocytes has been reported since then (Veeck *et al*., 1983; Prins *et al*., 1987; Nagy *et al*., 1996; Liu *et al*., 1997; Jaroudi *et al*., 1997; Edirisinghe *et al*., 1997; Söderström-Anttila *et al.*, 2006; Shu-Chi *et al.,* 2006; Fadini *et al.*, 2012; Chang *et al.*, 2014).

When using controlled hormonal hyperstimulation in ART, the majority of oocytes retrieved from stimulated cycles (about 85–90%) are at the mature MII stage, whereas 10–15% of oocytes are immature, either in GV or MI stages (Van Steirteghem *et al.,* 1993; Strassburger *et al.,* 2010). It has been shown that these oocytes can undergo spontaneous nuclear maturation *in vitro*, and then normal

fertilization and development. The improvement of oocyte culture strategies impacts maturation and fertilization rates, allowing a more efficient treatment. In fact, improved maturation and fertilization rates have been demonstrated by the inclusion of HMG in the culture medium for immature human oocytes (Prins *et al.,* 1987; Table I). It has been noted that the majority of immature oocytes reach the final stage of nuclear maturation by undergoing spontaneous nuclear maturation 24 hours after they were retrieved (Combelles *et al.*, 2002).

Moreover, immature oocytes obtained from patients undergoing gynaecological surgery, ovulation induction or having polycystic ovary syndrome (PCOS) can also be matured and fertilized *in vitro*, with about 80% of immature oocytes maturing to MII when they are cultured in maturation medium supplemented with gonadotropins (Cha and Chian, 1998), expanding the scope of fertility treatments.

Some of the causes for the failure to resume meiosis *in vivo*, with the consequent retrieval of immature oocytes arrested at the MI stage, might be an incomplete or absent LH effect, derangements in the signalling mechanism between oocyte and cumulus cells or intrinsic oocyte factors (Coticchio *et al.,* 2015). Focusing on intrinsic factors, MI arrest could be due to loss of the meiotic checkpoint where MPF, a metaphase (M-phase)-specific kinase, would remain inactivate; or it could be due to abnormal spindle formation (Mehlmann, 2005; Madgwick and Jones, 2007). Other authors suggested as causes for this arrest cytoplasmic incompetence, loss of MPF activation, disruption of factors involved in meiotic recombination and cytoskeleton anomalies as causes for this arrest (Mrazek and Fulka, 2003; Mehlmann, 2005; Madgwick and Jones, 2007; Coticchio *et al.,* 2015). Furthermore, specific arrest at MI might be caused by defects in the signal transduction pathway that mediates meiotic progression or abnormalities in the meiotic spindle (Beall *et al.,* 2010). Mutations in genes like *TUBB8*, whose expressed protein is a member of the meiotic spindle microtubules, and *PATL2*, whose expressed protein is related to topoisomerase II, a critical enzyme involved in DNA replication, have also been related to oocyte maturation arrest (Feng *et al.,* 2016; Chen *et al.,* 2017a,b).

Some reports have shown contradictory results when using MI oocytes in intracytoplasmic sperm injection (ICSI) treatments. One case revealed that MI oocytes, retrieved after ovarian stimulation, were devoid of *in vitro* maturation capacity. Ultrastructural analysis showed disrupted spindle formation in the presence of a conserved cytoplasm morphology (Windt *et al.,* 2001). Another report, with recurrent retrieval of MI oocytes after ovarian stimulation, also revealed that MI oocytes were unable to mature *in vitro* (Levran *et al.*, 2002). However, other cases revealed evidence that some MI oocytes could mature *in vitro* and be used for ICSI treatments. After microinjection of MI oocytes, higher degeneration rates, lower fertilization rates and higher rates of multinucleated zygotes were observed when compared to MII oocytes, but some attained the embryo cleavage stage. After transferring these embryos, a successful pregnancy and birth of a healthy newborn with a normal karyotype was achieved (Strassburger *et al.*, 2004).

Thus, as *in vitro* fertilization of matured MI oocytes can result in normal embryos and pregnancy, these oocytes should not be discarded, especially when few MII oocytes are retrieved (Vanhoutte, 2005; Álvarez *et al.*, 2013). However, embryos originated from MI oocytes can have higher rates of chromosomal aneuploidy (Strassburger *et al.*, 2010).

All these data highlight the clinical relevance of the knowledge on oocyte maturation processes, such as morphology and functional pathways of immature oocytes.

Throughout the years, the morphology of human oocytes has been reported by several authors, shedding some light on their ultrastructure at different developmental stages (Hertig and Adams, 1967; Sundstrom, 1985a,b; Sathananthan, 1985; Yang *et al.*, 2009; Morimoto, 2009; Shahedi *et al.*, 2013; Coticchio *et al.*, 2016; Palmerini *et al.*, 2014; Sousa *et al.*, 2016; Segovia *et al.*, 2017). However, none of these studies was exclusively dedicated to human MI oocytes.

The ultrastructural features of MI oocytes reported in previous studies were here corroborated, including the presence of areas devoid of organelles (Sundström *et al.*, 1985a; Motta *et al.*, 1988), of a narrow perivitelline space, of long and narrow microvilli, and of coated-vesicles and coated-pits (Zamboni and Thompson, 1972; Sundström *et al.*, 1985a,b; El Shafie *et al.*, 2000; Sathanathan, 2000, 2003). Dense cortical vesicles forming a continuous row under the oolema were noted, as well as a few isolated cortical vesicles in the subcortex and inner ooplasm, which is also similar to previous reports (Zamboni and Thompson, 1972; Sundström *et al.*, 1985a,b; El Shafie *et al.*, 2000; Sathanathan, 2000, 2003). Mitochondria were mainly oval and varied in size, with a moderately dense matrix and thin and dense *cristae*, mostly perpendicular to the organelle long axis. Some mitochondria were isolated, some were part of aggregates, and some were associated with SER vesicles or tubules. In the oocyte cytoplasm, several SER components were observed: SER small vesicles, SER medium vesicles, SER large vesicles and SER isolated tubules, also in line with the literature (Zamboni and Thompson, 1972; Sundström *et al.*, 1985a,b; El Shafie *et al.*, 2000; Sathanathan, 2000, 2003). The presence of SER tubular aggregates and secondary lysosomes in MI oocytes has also been reported (Zamboni and Thompson, 1972; Sundström *et al.*, 1985a,b; El Shafie *et al.*, 2000; Sathanathan, 2003). In MI oocytes, *annulated lamellae*, rough endoplasmic reticulum *cisternae*, multivesicular bodies, lipid droplets or polyribosomes were not observed. The presence of primary lysosomes or peroxisomes cannot be excluded, as a cytochemical analyses was not performed.

Regarding the morphology of MI oocytes we here first describe the presence of medium sized vesicles containing dense granular materials, mostly found in the oocyte cortex. They appeared to expel their contents into the perivitelline space after fusing with the oolemma, with contents also apparently fusing with the ZP.

While this systematic qualitative analysis allowed the integration of previous reports, the quantitative analysis of organelle distribution in MI oocytes is innovative, as no studies on the stereological analysis of human MI oocytes were previously performed. The analysis of the inner

three-dimensional structure and organelle distribution by stereological analysis, using the same protocol as a previous study on GV oocytes (Pires-Luis *et al.,* 2016), allowed further comparison between GV and MI oocytes.

The present stereological analysis in MI oocytes revealed that the organelles presenting the highest mean relative volumes were mitochondria (Vv = 6.5%) and total SER vesicles and tubules (Vv = 15.05%), similarly to GV oocytes. These organelles were somewhat equally distributed across the three oocyte regions (cortex, subcortex and inner ooplasm), with the relative volume of mitochondria being higher in the subcortex and the relative volume of total SER vesicles and tubules being slightly higher in the cortex, although not attaining statistically significant differences. Regarding mitochondria, it contrasts with mitochondria polarization in the subcortex and inner ooplasm observed at GV stage, although no statistical differences were found in the relative volume occupied by mitochondria in GV and MI oocytes ($P = 0.089$).

In what concerns the SER, it should be noted that SER-IT, SER-MV and SER-SV appeared evenly distributed throughout all oocyte regions in MI oocytes. Only SER-LV presented a statistically higher relative volume in the inner ooplasm (compared to the cortex). This was not observed in GV oocytes, where SER very large vesicles, absent in MI oocytes, presented significant higher Vv in the inner ooplasm. In parallel, the relative volume of total SER (excluding the very large vesicles specific of GV oocytes) was significantly higher in MI than in GV oocytes. Remarkably, the largest variation was noted for the volume of SER-IT, significantly higher in the MI cortex ($P = 0.005$), subcortex ($P = 0.003$) and inner cytoplasm ($P = 0.003$) than in GV counterparts. Additionally, the aggregates of SER tubules (aSERT) associated with mitochondria, which predominated in the cortex and subcortex of MI oocytes, were not depicted in GV oocytes. All this suggests an intensive remodelling of the SER compartment, from very large vesicles polarized in the inner cytoplasm at GV stage, to smaller SER elements evenly distributed at the MI stage. Of these, SER-LV were predominantly found in the inner ooplasm and aSERT were most frequent in the oocyte cortex and subcortex.

Cortical vesicles were mostly observed in the oocyte cortex (under the oolema), presenting a significantly higher relative volume in the cortex both in MI oocytes (cortex > subcortex and inner ooplasm) and in GV oocytes. This was expected in MI oocytes (Mao *et al.,* 2014).

The newly described medium sized vesicles containing dense granular materials, presented a relative volume is significantly higher in the cortex of MI oocytes ($P = 0.005$). In GV oocytes, larger and irregular vesicles also containing granular materials were also putatively observed to suffer exocytosis (Pires-Luis *et al.,* 2016). It is here speculated that in both immature oocytes, these vesicles might be involved in ZP maintenance.

Dictyosomes were rarely observed in MI oocytes, and the relative volume they occupied was significantly lower ($P < 0.001$) in oocytes at the MI stage (Vv = 0.01) compared to GV stage oocytes

(Vv = 0.5). As this organelle is involved in cortical vesicle formation, this might reflect a lower cortical vesicle formation rate at the oocyte MI stage.

Large secondary lysosomes, which indicate autophagy and an active metabolism in MI oocytes, were often found throughout the whole oocyte, with no significant differences ($P = 0.754$) among the three MI oocyte regions. Additionally, no significant difference was detected in the relative volume occupied by lysosomes between GV and MI oocytes.

The main limitation of the present study was the small number of MI oocytes evaluated (five), a problem not surpassed mostly due to the low availability of MI oocytes at ART facilities. Notwithstanding, a thorough quantitative evaluation was performed and the oocytes were retrieved from five different patients, allowing for a more heterogeneous sample.

This qualitative and quantitative evaluation might be useful in understanding the cellular mechanisms underlying oocyte maturation, especially GV to MI maturation. Correlation between morphological changes and functional data is warranted, as well as integration with expression analysis changes during maturation. Moreover, a similar analysis in mature oocytes arrested in MII would be useful to fully picture the morphological changes underlying oocyte cytoplasmic maturation. This may be important for the development of new *in vitro* oocyte maturation methods, more efficient and safe.

Chapter 5 – Conclusion

The aim of this study was to analyse metaphase-I human oocytes qualitatively and quantitatively, as well as to compare human prophase-I (GV) and metaphase-I (MI) arrested oocytes.

For the first time, medium sized vesicles containing dense granular materials (VZ) were described. Stereological analysis revealed that mitochondria and SER were the organelles with higher relative volumes at the MI stage, similarly to the GV stage. Cortical vesicles and VZ were mostly observed in the cortex and SER large vesicles were mostly observed in the inner ooplasm of MI oocytes. Additionally, data suggests an extensive SER remodelling from GV to MI stage.

Stereological analysis of metaphase-II oocytes and a combination of quantitative data on prophase-I, metaphase-I and metaphase-II oocytes, along with molecular data on oocyte maturation, will allow for a better understanding of human oocyte development and for a more effective design for future protocols of oocyte *in vitro* maturation.

Chapter 6 – Bibliography

Álvarez C, García-Garrido C, Taronger R and González de Merlo G (2013) In vitro maturation, fertilization, embryo development & clinical outcome of human metaphase-I oocytes retrieved from stimulated intracytoplasmic sperm injection cycles. *Indian J Med Res* **137**, 331-338.
PMID: 23563377

Baker TG (1963) A quantitative and cytological study of germ cells in human ovaries. *Proc R Soc Lond B Biol Sci* **158,** 417-433.
DOI: https://doi.org/10.1098/rspb.1963.0055

Beall S, Brenner C and Segars J (2010) Oocyte maturation failure: a syndrome of bad eggs. *Fertil Steril* **94,** 2507-2513.
DOI: https://doi.org/10.1016/j.fertnstert.2010.02.037

Bomsel-Helmreich O, Gougeon A, Thebault A, Saltarelli D, Milgrom E, Frydman R and Papiernik E (1979) Healthy and atretic human follicles in the preovulatory phase: differences in evolution of follicular morphology and steroid content of follicular fluid. *J Clin Endocrinol Metab* **48,** 686–694.
DOI: https://doi.org/10.1210/jcem-48-4-686

Cha K-Y and Chian R-C (1998) Maturation in vitro of immature human oocytes for clinical use. *Hum Reprod Update* **4,** 103-120.
DOI: https://doi.org/10.1093/humupd/4.2.103

Chang EM, Song HS, Lee DR, Lee WS and Yoon TK (2014) *In vitro* maturation of human oocytes: its role in infertility treatment and new possibilities. *Clin Exp Reprod Med* **41,** 41-46.
DOI: https://doi.org/10.5653/cerm.2014.41.2.41

Chen B, Li B, Li D, Yan Z, Mao X, Xu Y, Mu J, Li Q, Jin L, He L, Kuang Y, Sang Q and Wang L (2017a) Novel mutations and structural deletions in *TUBB8*: expanding mutational and phenotypic spectrum of patients with arrest in oocyte maturation, fertilization or early embryonic development. *Hum Reprod* **32,** 457-464.
DOI: https://doi.org/10.1093/humrep/dew322

Chen B, Zhang Z, Sun X, Kuang Y, Mao X, Wang X, Yan Z, Li B, Xu Y, Yu M, Fu J, Mu J, Zhou Z, Li Q, Jin L, He L, Sang Q and Wang L (2017b) Biallelic mutations in *PATL2* cause female infertility characterized by oocyte maturation arrest. *Am J Hum Genet* **101,** 609-615.
DOI: https://doi.org/10.1016/j.ajhg.2017.08.018

Combelles CMH, Cekleniak NA, Racowsky C and Albertini DF (2002) Assessment of nuclear and cytoplasmic maturation in in vitro matured human oocytes. *Hum Reprod* **17,** 1006-1016.
DOI: https://doi.org/10.1093/humrep/17.4.1006

Conti M and Franciosi F (2018) Acquisition of oocyte competence to develop as an embryo: integrated nuclear and cytoplasmic events. *Hum Reprod Update* **24,** 245-266.
DOI: https://doi.org/10.1093/humupd/dmx040

Coticchio G, Dal Canto M, Renzini MM, Guglielmo MC, Brambillasca F, Turchi D, Novara PV and Fadini R (2015) Oocyte maturation: gamete-somatic cell interactions, meiotic resumption, cytoskeletal dynamics and cytoplasmic reorganization. *Hum Reprod Update* **21,** 427-454.
DOI: https://doi.org/10.1093/humupd/dmv011

Coticchio G, Dal Canto M, Fadini R, Renzini MM, Guglielmo MC, Miglietta S, Palmerini MG, Macchiarelli G and Nottola SA (2016) Ultrastructure of human oocytes after in vitro maturation. *Mol Hum Reprod* **22,** 110-118.
DOI: https://doi.org/10.1093/molehr/gav071

DiLuigi A, Weitzman VN, Pace MC, Siano LJ, Maier D and Mehlmann LM (2008) Meiotic arrest in human oocytes is maintained by a Gs signaling pathway. *Biol Reprod* **78,** 667–672.
DOI: https://doi.org/10.1095/biolreprod.107.066019

Dunlop CE and Anderson RA (2014) The regulation and assessment of follicular growth. *Scand J Clin Lab Inv* **74** (Suppl. 244), 13-17.
DOI: https://doi.org/10.3109/00365513.2014.936674

Duran HE, Simsek-Duran F, Oehninger SC, Jones HW Jr and Castora FJ (2011) The association of reproductive senescence with mitochondrial quantity, function, and DNA integrity in human oocytes at different stages of maturation. *Fertil Steril* **96,** 384-388.
DOI: https://doi.org/10.1016/j.fertnstert.2011.05.056

Edirisinghe WR, Junk SM and Matson PL and Yovich JL (1997) Birth from cryopreserved embryos following in vitro maturation of oocytes and intracytoplasmic sperm injection. *Hum Reprod* **12,** 1056-1058.
DOI: https://doi.org/10.1093/humrep/12.5.1056

Edwards RG (1974) Follicular fluid. *J Reprod Fertil* (*Reproduction*) **37,** 189-219.
DOI: https://doi.org/10.1530/jrf.0.0370189

Edwards RG (1965a) Maturation in vitro of mouse, sheep, cow, pig, rhesus monkey and human ovarian oocytes. *Nature* **208,** 349-351.
DOI: https://doi.org/10.1038/208349a0

Edwards RG (1965b) Maturation in vitro of human ovarian oocytes. *Lancet* **286,** 926-929.
DOI: http://dx.doi.org/10.1016/S0140-6736(65)92903-X

Edwards RG, Bavister BD and Steptoe PC (1969) Early stages of fertilization in vitro of human oocytes matured in vitro. *Nature* **221,** 632–635.
DOI: https://doi.org/10.1038/221632a0

El Shafie M, Windt M-L, Kitshoff M, McGregor P, Sousa M, Wranz PAB and Kruger TF (2000) Ultrastructure of human oocytes: a transmission electron microscopy view. *In: An Atlas of the ultrastructure of human oocytes: a guide for assisted reproduction.* El Shafie M, Windt M-L, Sousa M, Kruger TF (Eds). Chapter 6, The Parthenon Publishing Group, NY, USA. p: 83-173.
ISBN-10:185070404X

Erickson GF (1986) An analysis of follicle development and ovum maturation. *Semin Reprod Endocrinol* **4,** 233-254.
DOI: https://doi.org/10.1055/s-2007-1022504

Erickson GF (2008) Follicle Growth and Development. *Glob libr women's med* (ISSN: 1756-2228)
DOI: https://doi.org/10.3843/GLOWM.10289

Fadini R, Mignini Renzini M, Guarnieri T, Dal Canto M, De Ponti E, Sutcliffe A, Shevlin M, Comi R, Coticchio G (2012) Comparison of the obstetric and perinatal outcomes of children conceived from in vitro or in vivo matured oocytes in in vitro maturation treatments with births from conventional ICSI cycles. *Hum Reprod* **27,** 3601-3608

DOI: https://doi.org/10.1093/humrep/des359

Feng R, Sang Q, Kuang Y, Sun X, Yan Z, Zhang S, Shi J, Tian G, Luchniak A, Fukuda Y, Li B, Yu M, Chen J, Xu Y, Guo L, Qu R, Wang X, Sun Z, Liu M, Shi H, Wang H, Feng Yi, Shao R, Chai R, Li Q, Xing Q, Zhang R, Nogales E, Jin L, He L, Gupta ML Jr, Cowan NJ and Wang L (2016) Mutations in *TUBB8* and human oocyte meiotic arrest. *N Engl J Med* **374,** 223-232.
DOI: https://doi.org/10.1056/NEJMoa1510791

Ferrer-Buitrago M, Dhaenens L, Lu Y, Bonte D, Vanden Meerschaut F, De Sutter P, Leybaert L and Heindryckx B (2018) Human oocyte calcium analysis predicts the response to assisted oocyte activation in patients experiencing fertilization failure after ICSI. *Hum Reprod* **33,** 416-425.
DOI: https://doi.org/10.1093/humrep/dex376

Furcila D, Domínguez-Álvaro M, DeFelipe J and Alonso-Nanclares L (2019) Subregional density of neurons, neurofibrillary tangles and amyloid plaques in the hippocampus of patients with Alzheimer's Disease. *Front Neuroanat* **13,** 99.
DOI: https://doi.org/10.3389/fnana.2019.00099

Gougeon A (1998) Ovarian follicular growth in humans: ovarian ageing and population of growing follicles. *Maturitas* **30,** 137-142.
DOI: https://doi.org/10.1016/s0378-5122(98)00069-3

Gundersen HJG and Jensen EB (1987) The efficiency of systematic sampling in stereology and its prediction. *J Microsc* **147,** 229-263.
DOI: https://doi.org/10.1111/j.1365-2818.1987.tb02837.x

Gundersen HJG, Bendtsen TF, Korbo L, Marcussen N, Møller A, Nielsen K, Nyengaard Jr, Pakkenberg B, Sørensen FB, Vesterby A and West MJ (1988) Some new, simple and efficient stereological methods and their use in pathological research and diagnosis. *APMIS* **96,** 379-394.
DOI: https://doi.org/10.1111/j.1699-0463.1988.tb05320.x

Hertig AT and Adams EC (1967) Studies on the human oocyte and its follicle. *J cell Biol* **34,** 647-675.
DOI: https://doi.org/10.1083/jcb.34.2.647

Hou Y, Fan W, Yan L, Li R, Lian Y, Huang J, Li J, Xu L, Tang F, Xie XS and Qiao J (2013) Genome analyses of single human oocytes. *Cell* **155,** 1492-1506.
DOI: https://doi.org/10.1016/j.cell.2013.11.040

Howard CV and Reed MG (2005) Unbiased Stereology: Three dimensional measurement in microscopy (advanced methods). Chapter 1, Garland Science/BIOS Scientific Publishers, Abingdon, UK. p: 12.
ISBN-10: 1859960898

Jaroudi KA, Hollanders JM, Sieck UV, Roca GL, El-Nour AM and Coskun S (1997) Pregnancy after transfer of embryos which were generated from in-vitro matured oocytes. *Hum. Reprod* **12,** 857–859.
DOI: https://doi.org/10.1093/humrep/12.4.857

Jones KT (2004) Turning it on and off: M-phase promoting factor during meiotic maturation and fertilization. *Mol Hum Reprod* **10,** 1-5.
DOI: https://doi.org/10.1093/molehr/gah009

Jones KT (2005) Mammalian egg activation: from Ca^{2+} spiking to cell cycle progression. *Reproduction* **130,** 813-823.
DOI: https://doi.org/10.1530/rep.1.00710

Kim B, Park JY, Cho DY, Ko HM, Yoon SH and Choi DK (2020) 2-(5-(4-Chlorophenyl)-1-(2,4-dichlorophenyl)-4-methyl-1H-pyrazol-3-yl)-N-(2-hydroxyethyl)-2-oxoacetamide (CDMPO) has anti-inflammatory properties in microglial cells and prevents neuronal and behavioral deficits in MPTP mouse model of Parkinson's disease. *Neuropharmacology* **166,** 107928.
DOI: https://doi.org/10.1016/j.neuropharm.2019.107928

Kipanyula MJ and Sife AS (2018) Global trends in application of stereology as a quantitative tool in biomedical research. *BioMed Res Int* **2018,** 1-9.
DOI: https://doi.org/10.1155/2018/1825697

Levran D, Farhi J, Nahum H, Glezerman M and Weissman A (2002) Maturation arrest of human oocytes as a cause of infertility: case report. *Hum Reprod* **17,** 1604-1609.
DOI: https://doi.org/10.1093/humrep/17.6.1604

Li H and Chian R-C (2017) Follicular Development and Oocyte Growth. *In: Development of in vitro maturation for human oocytes.* Chian RC, Nargund G, Huang J (Eds). Springer, Cham. p: 37-57.
DOI: https://doi.org/10.1007/978-3-319-53454-1_2

Li Y, Liu H, Yu Q, Liu H, Huang T, Zhao S, Ma J and Zhao H (2019) Growth hormone promotes in vitro maturation of human oocytes. *Front Endocrinol* **10,** 485.
DOI: https://doi.org/10.3389/fendo.2019.00485

Liu C, Li M, Li T, Zhao H, Huang J, Wang Y, Gao Q, Yu Y and Shi Q (2016) *ECAT1* is essential for human oocyte maturation and pre-implantation development of the resulting embryos. *Sci Rep* **6,** 38192.
DOI: https://doi.org/10.1038/srep38192

Liu J, Katz E, Garcia JE, Compton G and Baramki TA (1997) Successful in vitro maturation of human oocytes not exposed to human chorionic gonadotropin during ovulation induction, resulting in pregnancy. *Fertil Steril* **67,** 566-568.
DOI: https://doi.org/10.1016/s0015-0282(97)80088-x

Madgwick S and Jones KT (2007) How eggs arrest at metaphase II: MPF stabilization plus APC/C inhibition equals Cytostatic Factor. *Cell Division* **2,** 4.
DOI: https://doi.org/10.1186/1747-1028-2-4

Mandarim-de-Lacerda CA (2003) Stereological tools in biomedical research. *An Acad Bras Cienc* **75,** 469-486.
DOI: https://doi.org/10.1590/s0001-37652003000400006

Mandelbaum J (2000) Oocytes. *Hum Reprod* **15** (Suppl. 4)**,** 11-18.
DOI: https://doi.org/10.1093/humrep/15.suppl_4.11

Mao L, Lou H, Lou Y, Wang N and Jin F (2014) Behaviour of cytoplasmic organelles and cytoskeleton during oocyte maturation. *Reprod BioMed Online* **28,** 284– 299.
DOI: https://doi.org/10.1016/j.rbmo.2013.10.016

Mehlmann LM (2005) Stops and starts in mammalian oocytes: recent advances in understanding the regulation of meiotic arrest and oocyte maturation. *Reproduction* **130,** 791-799.

DOI: https://doi.org/10.1530/rep.1.00793

Meyer TE and Habener JF (1993) Cyclic adenosine 3',5'-monophosphate response element binding protein (CREB) and related transcription-activating deoxyribonucleic acidbinding proteins. *Endocr Rev* **14,** 269-290.
DOI: https://doi.org/10.1210/edrv-14-3-269

Morimoto Y (2009) Ultrastructure of the human oocytes during in vitro maturation. *J Mamm Ova Res* **26,** 10-17.
DOI: https://doi.org/10.1274/jmor.26.10

Motta PM, Nottola SA, Micara G and Familiari G (1988) Ultrastructure of human unfertilized oocytes and polyspermic embryos in an IVF-ET program. *Ann N Y Acad Sci* **541,** 367-383.
DOI: https://doi.org/10.1111/j.1749-6632.1988.tb22274.x

Mrazek M and Fulka J Jr (2003) Failure of oocyte maturation: possible mechanisms for oocyte maturation arrest. *Hum Reprod* **18,** 2249-2252.
DOI: https://doi.org/10.1093/humrep/deg434

Nagy ZP, Cecile J, Liu J, Loccufier A, Devroey P, and Van Steirteghem A (1996) Pregnancy and birth after intracytoplasmic sperm injection of in vitro matured germinal-vesicle stage oocytes: case report. *Fertil Steril* **65,** 1047-1050.
DOI: https://doi.org/10.1016/s0015-0282(16)58285-5

Nogueira D, Ron-El R, Friedler S, Schachter M, Raziel A, Cortvrindt R and Smitz J (2006) Meiotic arrest in vitro by phosphodiesterase 3-inhibitor enhances maturation capacity of human oocytes and allows subsequent embryonic development. *Biol Reprod* **74,** 177-184.
DOI: https://doi.org/10.1095/biolreprod.105.040485

Okutsu Y, Itoh MT, Takahashi N and Ishizuka B (2010) Exogenous androstenedione induces formation of follicular cysts and premature luteinization of granulosa cells in the ovary. *Fertil Steril* **93,** 927–935.
DOI: https://doi.org/10.1016/j.fertnstert.2008.10.064

Orisaka M, Tajima K, Tsang BK and Kotsuji F (2009) Oocyte-granulosa-techa cell interactions during preantral follicular development. *J Ovarian Res* **2,** 9.

DOI: https://doi.org/10.1186/1757-2215-2-9

Paldino E, Balducci C, La Vitola P, Artioli L, D'Angelo V, Giampà C, Artuso V, Forloni G and Fusco FR (2019) Neuroprotective Effects of Doxycycline in the R6/2 Mouse Model of Huntington's Disease. *Mol Neurobiol.*
DOI: https://doi.org/10.1007/s12035-019-01847-8

Palmerini MG, Antinori M, Maione M, Cerusico F, Versaci C, Nottola SA, Macchiarelli G, Khalili MA and Antinori S (2014) Ultrastructure of immature and mature human oocytes after cryotop vitrification. *J Reprod Dev* **60,** 411-420.
DOI: https://doi.org/10.1262/jrd.2014-027

Pires-Luís AS, Rocha E, Bartosch C, Oliveira E, Silva J, Barros A, Sá R and Sousa M (2016) A stereological study on organelle distribution in human oocytes at prophase I. *Zygote* **24,** 346-354.
DOI: https://doi.org/10.1017/S0967199415000258

Prins GS, Wagner C, Weidel L, Gianfortoni J, Marut EL and Scommegna A (1987) Gonadotropins augment maturation and fertilization of human immature oocytes cultured in vitro. *Fertil Steril* **47,** 1035–1037.
DOI: https://doi.org/10.1016/s0015-0282(16)59243-7

Sá R and Sousa M (2014). Androgens and the ovary. *In: Androgen Receptors*. Socorro S (Ed). Chapter 7. Nova Science Publishers, Inc. NY, USA. p: 166-190.
ISBN: 978-1-62948-693-2

Sagheb HRM and Moudi B (2014) Basic Application of Stereology in Histology and Medical Sciences. *Gene Cell Tissue* **1:** e24237.
DOI: https://doi.org/10.17795/gct-24237

Sánchez F and Smitz J (2012) Molecular control of oogenesis. *Biochim Biophys Acta* **1822,** 1896-1912.
DOI: https://doi.org/10.1016/j.bbadis.2012.05.013

Sathananthan AH (1985) Maturation of the human oocyte in vitro: nuclear events during meiosis (an ultrastructural study). *Gamete Res* **12,** 237-254.
DOI: https://doi.org/10.1002/mrd.1120120303

Sathananthan AH (1994) Ultrastructural changes during meiotic maturation in mammalian oocytes: unique aspects of the human oocyte. *Microsc Res Tech* **27,** 145-164.
DOI: https://doi.org/10.1002/jemt.1070270208

Sathananthan AH (2000) Ultrastructure of human gametes, fertilization, and embryo development. *In: Handbook of in vitro fertilization.* Trouson AO, Gardner DK (Eds). Chapter 18, 2nd edition, CRC Press LLC, Boca Raton, FL, USA. p: 431-464.
ISBN 0-8493-4002-0

Sathananthan AH (2003) Morphology and pathology of the human oocyte. *In: Biology and pathology of the oocyte.* Trouson AO, Gosden RG (Eds). Chapter 13, 1st edition, Cambridge University Press, Cambridge, UK. p: 185-208.
ISBN 0-521-79958-9

Sedmak G and Judas M (2019) The total number of white matter interstitial neurons in the human brain. *J Anat* **235,** 626-636.
DOI: https://doi.org/10.1111/joa.13018

Segovia Y, Victory N, Peinado I, García-Valverde LM, García M, Aizpurua J, Monzó A and Gómez-Torres MJ (2017) Ultrastructural characteristics of human oocytes vitrified before and after in vitro maturation. *J Reprod Dev* **63,** 377-382.
DOI: https://doi.org/10.1262/jrd.2017-009

Sen A and Caiazza F (2013) Oocyte Maturation: A story of arrest and release. *Front Biosci (Schol Ed)* **S5,** 451-477.
DOI: https://doi.org/10.2741/S383

Shahedi A, Khalili MA, Soleimani M and Morshedizad S (2013) Ultrastructure of in vitro matured human oocytes. *Iran Red Crescent Med J* **15,** e7379.
DOI: https://doi.org/10.5812/ircmj.7379

Shu-Chi M, Jiann-Loung H, Yu-Hung L, Tseng-Chen S, Ming-I L and Tsu-Fuh Y (2006) Growth and development of children conceived by in-vitro maturation of human oocytes. *Early Hum Dev* **82,** 677-682.
DOI: https://doi.org/10.1016/j.earlhumdev.2006.01.012

Söderström-Anttila V, Salokorpi T, Pihlaja M, Serenius-Sirve S and Suikkari AM (2006) Obstetric and perinatal outcome and preliminary results of development of children born after in vitro maturation of oocytes. *Hum Reprod* **21,** 1508-1513.
DOI: https://doi.org/10.1093/humrep/dei503

Sousa M, Barros A, Silva J and Tesarik J (1997) Developmental changes in calcium content of ultrastructurally distinct subcellular compartments of preimplantation human embryos. *Mol Hum Reprod* **3,** 83-90.
DOI: https://doi.org/10.1093/molehr/3.2.83

Sousa M and Tesarik J (1994) Ultrastructural analysis of fertilization failure after intracytoplasmic sperm injection. *Hum Reprod* **9,** 2374-2380.
DOI: https://doi.org/10.1093/oxfordjournals.humrep.a138455

Sousa M, Oliveira E, Barros N, Barros A and Sá R (2016) New ultrastructural observations of human oocyte smooth endoplasmic reticulum tubular aggregates and cortical reaction: update on the molecular mechanisms involved. *Rev Int Androl* **14,** 113-122.
DOI: https://doi.org/10.1016/j.androl.2016.04.005

Steptoe PC and Edwards RG (1978) Birth after the reimplantation of a human embryo. *Lancet* **312,** 366.
DOI: https://doi.org/10.1016/s0140-6736(78)92957-4

Strassburger D, Friedler S, Raziel A, Kasterstein E, Schachter M and Ron-El R (2004) The outcome of ICSI of immature MI oocytes and rescued *in vitro* matured MII oocytes. *Hum Reprod* **19,** 1587-1590.
DOI: https://doi.org/10.1093/humrep/deh236

Strassburger D, Goldstein A, Friedler S, Raziel A, Kasterstein E, Mashevich M, Schachter M, Ron-El R and Reish O (2010) The cytogenic constitution of embryos derived from immature (metaphase I) oocytes obtained after ovarian hyperstimulation. *Fertil Steril* **94,** 971-978.
DOI: https://doi.org/10.1016/j.fertnstert.2009.04.035

Sundström P, Nilsson BO, Liedholm P and Larsson E (1985a) Ultrastructural characteristics of human oocytes fixed at follicular puncture or after culture. *J In Vitro Fert Embryo Transf* **2,** 195-206.

DOI: https://doi.org/10.1007/bf01201797

Sundström P, Nilsson BO, Liedholm P and Larsson E (1985b) Ultrastructure of maturing human oocytes. *Ann N Y Acad Sci* **442,** 324-331.
DOI: https://doi.org/10.1111/j.1749-6632.1985.tb37536.x

Thibault C, Gerard M and Menezo Y (1975) Preovulatory and ovulatory mechanisms in oocyte maturation. *J Reprod Fertil* **45,** 605-610.
DOI: https://doi.org/10.1530/jrf.0.0450605

Van Steirteghem AC, Liu J, Joris H, Nagy Z, Janssenswillen C, Tournaye H, Derde MP, Van Assche E and Devroey P (1993) Higher success rate by intracytoplasmic sperm injection than by subzonal insemination. Report of a second series of 300 consecutive treatment cycles. *Hum Reprod* **8,** 1055-1060.
DOI: https://doi.org/10.1093/oxfordjournals.humrep.a138191

Vanhoutte L, De Sutter P, Van der Elst J and Dhont M (2005) Clinical benefit of metaphase I oocytes. *Reprod Biol Endocrinol* **3,** 71.
DOI: https://doi.org/10.1186/1477-7827-3-71

Veeck LL, Wortham JW Jr, Witmyer J, Sandow BA, Acosta AA, Garcia JE, Jones GS and Jones HW Jr (1983) Maturation and fertilization of morphologically immature human oocytes in a program of in vitro fertilization. *Fertil Steril* **39,** 594-602.
DOI: https://doi.org/10.1016/s0015-0282(16)47052-4

Virant-Klun I, Knez K, Tomazevic T and Skutella T (2013) Gene expression profiling of human oocytes developed and matured *in vivo* or *in vitro*. *Biomed Res Int* **2013.**
DOI: https://doi.org/10.1155/2013/879489

Virant-Klun I, Leicht S, Hughes C and Krijgsveld J (2016) Identification of maturation-specific proteins by single-cell proteomics of human oocytes. *Mol Cell Proteomics* **15,** 2616-2627.
DOI: https://doi.org/10.1074/mcp.M115.056887

Watson AJ (2007) Oocyte cytoplasmic maturation: a key mediator of oocyte and embryo developmental competence. *J Anim Sci* **85,** E1-E3.
DOI: https://doi.org/10.2527/jas.2006-432

Weibel ER, Kistler GS and Scherle WF (1966) Practical stereological methods for morphometric cytology. *J Cell Biol* **30,** 23-38.
DOI: https://doi.org/10.1083/jcb.30.1.23

Windt ML, Coetzee K, Kruger TF, Marino H, Kitshoff MS and Sousa M (2001) Ultrastructural evaluation of recurrent and in-vitro maturation resistant metaphase I arrested oocytes. *Hum Reprod* **16,** 2394-2398.
DOI: https://doi.org/10.1093/humrep/16.11.2394

Wood JR, Dumesic DA, Abbott DH and Strauss JF 3rd (2007) Molecular abnormalities in oocytes from woman with polycystic ovary syndrome revealed by microarray analysis. *J Clin Endocrinol Metab* **92,** 705-713.
DOI: https://doi.org/10.1210/jc.2006-2123

Yang YJ, Zhang YJ and Li Y (2009) Ultrastructure of human oocytes of different maturity stages and the alteration during in vitro maturation. *Fertil Steril* **92,** 396.e1-e6.
DOI: https://doi.org/10.1016/j.fertnstert.2009.02.010

Yu B, Dong X, Gravina S, Kartal Ö, Schimmel T, Cohen J, Tortoriello D, Zody R, Hawkins RD and Vijg J (2017) Genome-wide, single-cell DNA methylomics reveals increased non-CpG methylation during human oocyte maturation. *Stem Cell Rep* **9,** 397-407.
DOI: https://doi.org/10.1016/j.stemcr.2017.05.026

Zamboni L, Thompson RS and Smith DM (1972) Fine morphology of human oocyte maturation in vitro. *Biol Reprod* **7,** 425-457.
DOI: https://doi.org/10.1093/biolreprod/7.3.425

Zhao H, Li T, Zhao Y, Tan T, Liu C, Liu Y, Chang L, Huang N, Li C, Fan Y, Yu Y, Li R and Qiao J (2019) Single-cell transcriptomics of human oocytes: environment-driven metabolic competition and compensatory mechanisms during oocyte maturation. *Antioxid Redox Signal* **30,** 542-559.
DOI: https://doi.org/10.1089/ars.2017.7151